UNSTEADY NATURAL CONVECTION IN CYLINDRICAL ENCLOSURES WITH STRATIFIED MEDIUM

BY

RUEY-JONG SHYU

A DISSERTATION PRESENTED TO THE GRADUATE SCHOOL
OF THE UNIVERSITY OF FLORIDA IN
PARTIAL FULFILLMENT OF THE REQUIREMENTS
FOR THE DEGREE OF DOCTOR OF PHILOSOPHY

UNIVERSITY OF FLORIDA

1985

To My Parents

ACKNOWLEDGMENTS

The author wishes to express his sincere appreciation to his graduate supervisory committee, which includes Drs. C.K. Hsieh, Chairman, R.A. Gater, E.C. Hansen, Tom I.P. Shih, and C.C. Hsu. Special thanks go to his adviser, Dr. C.K. Hsieh, without whose excellent guidance and helpful advice this work would not have been possible.

The author also wishes to thank his wife, Chie-Jo. Her encouragement and support made his graduate study a beautiful memory.

Finally, the author wishes to acknowledge the support of the Interactive Graphics Laboratory (IGL) at the University of Florida for providing free computer time and graphics facilities.

TABLE OF CONTENTS

Page

ACKNOWLEDGMENTS iii

LIST OF TABLES vii

LIST OF FIGURES viii

NOMENCLATURE xi

ABSTRACT xv

CHAPTERS

I INTRODUCTION 1

II LITERATURE REVIEW 3

2.1 Natural Convection in Enclosures 3
2.1.1 Differentially Heated Conditions 5
2.1.2 Symmetrically Heated Conditions 8
2.2 Energy Storage in a Thermocline or a Stratified Medium 10

III MATHEMATICAL FORMULATION 15

3.1 Governing Equations and Conditions for Natural Convection in Water 17
3.2 Governing Equations and Conditions for Heat Conduction in Wall 22

IV METHODS OF SOLUTION 25

4.1 Special Treatment in the Solution 25
4.1.1 Computation of Heat Loss from Wall to the Ambient Air 25
4.1.2 Matching of Conditions at Wall/Water and Wall/Insulation Interfaces 30
4.1.3 Kinmetically Consistent Velocity Fields 33
4.1.4 Generation of Nonuniform Grid System 40
4.2 Solution Strategy 43

V FINITE DIFFERENCE EQUATIONS FOR GOVERNING EQUATIONS AND BOUNDARY CONDITIONS 47

5.1 Finite-Difference Formulation for Energy Equation in Wall 47
5.1.1 Bare Wall 50
5.1.2 Insulated Wall 55
5.1.3 Summary in Matrix Forms 61
5.2 Finite-Difference Formulation for Energy Equation in Water 66
5.3 Iterative Solution for Two Energy Equations 75
5.4 Finite-Difference Formulation for Vorticity Transport Equation 76
5.5 Finite-Difference Formulation for Stream Function Equation 84
5.6 Solution Algorithm 85

VI RESULTS AND DISCUSSION 87

6.1 Flow and Temperature Fields in Water for Different Designs of the Wall 88
6.1.1 Uninsulated Tank 89
6.1.2 Tank Insulated from the Outside 93
6.1.3 Tank Insulated at the Inside 99
6.2 Heat Fluxes at Wall/Water Interface 99
6.2.1 Heat Flux Distribution for A1 Case 105
6.2.2 Heat Flux Distribution for E1 Case 105
6.2.3 Heat Flux Distribution for I1 Case 108
6.3 Convective Coefficients at the Air Side 108
6.4 Velocity and Temperature Distributions in the Boundary Region 113
6.5 Flow Reversal and Temperature Defect 118
6.6 Energy Analysis 127
6.7 Evaluation of Stratification Index 132

VII REMARKS ON NUMERICAL RESULTS 134

7.1 Effect of Time-Step Size on Stability and Convergence 134
7.2 Effect of Grid Size on Convergence 137
7.3 Test of Convergence Criteria for Vorticities 140

VIII CONCLUSIONS AND RECOMMENDATIONS 145

APPENDICES

A PHYSICAL PROPERTIES 148

B TIME SCALE ANALYSIS FOR DETERMINING HEAT TRANSFER MECHANISMS 149

REFERENCES 163
BIOGRAPHICAL SKETCH 169

LIST OF TABLES

Table		Page
4.1	Comparison of exact solution and approximate solution for heat loss calculation	29
4.2	Weighting coefficients in equation (4.20)	38
5.1	Definitions for C coefficients	52
6.1	Comparison between numerical and experimental data	119
7.1	CPU time consumed for different time steps calculated up to 60 seconds' cooling time	138

LIST OF FIGURES

Figure		Page
2.1	Natural convection in enclosures	4
3.1	Coordinate system and initial temperature distribution	16
4.1	Interface properties	32
4.2	Notations for an interior grid volume in a nonuniform cylindrical grid system	35
4.3	Stretching functions in z direction and r direction	42
4.4	Grid system in water used in the present study	44
5.1	Notation for control-volume method	49
5.2	Treatment of grid points adjacent to interface	56
5.3	Wall region temperature boundary conditions	60
5.4	Second upwind difference scheme	69
5.5	Water region temperature boundary conditions	71
5.6	Water region vorticity boundary conditions	79
6.1	Isotherm, velocity field, and streamline for tank without insulation	90
6.2	Centerline water temperature variation with time for tank without insulation	94
6.3	Isotherm, velocity field, and streamline for tank with exterior insulation	95
6.4	Centerline water temperature variation with time for tank with exterior insulation	98
6.5	Isotherm, velocity field, and streamline for tank with interior insulation	100

6.6 Centerline water temperature variation with time for tank with interior insulation. 104

6.7 Heat flux distribution for tank without insulation. 106

6.8 Heat flux distribution for tank with exterior insulation. 107

6.9 Heat flux distribution for tank with interior insulation. 109

6.10 Heat flux distribution for three designs of the wall at different times. 110

6.11 Heat transfer coefficients for three designs of the wall at different times. 112

6.12 Velocity profiles at various elevations at 60 seconds for three desiges of the wall. 114

6.13 Temperature profiles at various elevations at 60 seconds for three designs of the wall. 116

6.14 An enlarged view of the flow field in the lower section of the enclosure in Fig. 6.1(a). 120

6.15 Decomposition of velocity vectors into their z and r components. 121

6.16 Temperature and velocity profiles for Ni case at i = 11 grid line. 123

6.17 Boundary layers on a vertical, heated surface. 124

6.18 Determination of temperature defect region by comparing two temperature gradients. 126

6.19 Superposition of two sections of temperature profile to obtain velocity profiles. 128

6.20 Numerical errors evaluated for three cases based on the energy conservation principle. 130

6.21 Comparison of ability of walls to preserve energy in water. 131

6.22 Centerline water temperature profiles at 3 hours for three designs of the wall. 133

7.1 Iteration counts for convergence tests: (a) heat flux, (b) boundary vorticity. 136

7.2 Axial velocity profiles for various time-steps at 60 seconds.....139

7.3 Isotherm, velocity field, and streamline for different grid systems at 60 seconds.....141

7.4 Axial velocity profiles for different grid systems at 60 seconds.....142

7.5 Axial velocity profiles for three convergence criteria of the boundary vorticity.....143

8.1 Six time scales for six heat-transfer mechanisms.....150

8.2 Schematic diagrams for studying time scales.....153

NOMENCLATURE

A	aspect ratio, H/R_1
$\bar{\bar{A}}$	matrix
a	constant in equation (4.29)
B	HR_3/α^2
$\bar{B}$	vector
b	constant in equation (4.29)
C	constant in equation (4.4)
$\bar{C}$	vector
C_p	specific heat
C_9-C_{30}	coefficients in finite-difference equation defined in Table 5.1
C^*_{13}-C^*_{15}	coefficients in finite-difference equation defined in equation (5.11)
F	body force
F_B	fraction of enclosure height in equation (B.7)
F_f	fraction of enclosure height in equation (B.9)
F_S	fraction of enclosure height in equation (B.2)
g	gravity force
H	height of enclosure
h	heat transfer coefficient
k	thermal conductivity
l	perimeter of a control volume

n	constant in equation (4.1)
N	constant in equation (4.1)
P	pressure
Pr	Prandtl number
Q	total heat capacity
Q'	source term
q	heat flux
R	radius of enclosure
r	radial coordinate
Ra	Rayleight number, $g\beta H^3(T_{s,o} - T_\infty)/\alpha\nu$
S	stratification parameter
s	area of a control volume
T	temperature
t	time
Δt_c	critical time-step size
u	axial velocity
u_s, u_n	transport velocities in z direction
V	velocity
v	radial velocity
v_e, v_w	transport velocities in r direction
Δx	grid size
z	axial coordinate
α	thermal diffusivity
α_j	weighting coefficient in equation (4.20)
β	coefficient of expansion

a_j	weighting coefficient in equation (4.20)
δ	wall/insulation thickness, $R_o - R_i$
δ_T	thermal boundary layer thickness
δ_1, δ_2	thickness of components of velocity profile
δ_{T1}, δ_{T2}	thickness of components of temperature profile
η	transformation function in z direction
κ	iteration parameter in equation (5.36)
λ	relaxation factor in equation (5.44)
μ	dynamic viscosity
ν	kinematic viscosity
ξ	transformation function in r direction
ρ	density
Φ	viscous dissipation
ψ	stream function
ψ^*	stream function at corners of a control volume
ω	vorticity

superscript

k	time coordinate in finite difference representation
l	iteration index, also iteration counts
n	normal component
t	tangential component
*	nondimensional quantity

subscript

a	insulation, also ambient
b	boundary, also buoyancy
c	centerline, also convection

d	dynamic
f	fluid
i	inside, also interface
i,j	space coordinate in finite difference representation
j	element designation in z direction in equation (4.5)
n	normal direction
o	outside, also initial
r	radial component
s	solid, also surface
t	time
w	wall
z	axial component
∞	ambient air

Abstract of Dissertation Presented to the Graduate School of the University of Florida in Partial Fulfillment of the Requirements for the Degree of Doctor of Philosophy

UNSTEADY NATURAL CONVECTION IN CYLINDRICAL ENCLOSURES WITH STRATIFIED MEDIUM

BY

RUEY-JONG SHYU

August, 1988

Chairman: C. K. Hsieh
Major Department: Mechanical Engineering

A numerical study was given to investigate unsteady natural convection in enclosures with thermally stratified water. Two different designs of enclosure wall were analyzed, one placing insulation on the outside of the wall, the other placing the insulation over the inside of the wall. An uninsulated enclosure was also studied for use as control. For all the cases studied, water was stratified at the midsection of the enclosure; hot water occupied the top section, while cold water was located at the bottom section. The wall temperature was initially uniform at the hot-water temperature.

The problem was solved as a conjugate heat transfer problem to determine the flow and temperature fields in water and the temperature field in wall. In the numerical solution, the wall and the water were treated as two separate regions, and conditions were

derived for matching temperature and heat flux at the wall/water interface. The governing equations were transformed into a vorticity-stream function formulation, and control-volume approach was used to derive the finite-difference equations. The wall and water energy equations and the vorticity transport equation were solved by the use of Alternating Direction Implicit method, while the stream function equation was solved by the use of Successive Over-Relaxation method.

The numerical results indicate that exterior and interior insulation are about equal in preserving energy, however, the interior insulation performs far better in retaining stratification in water, an outcome that is highly desirable for solar/thermal energy-storage applications. The velocity and temperature fields in the boundary layer at the early stage of cooling were also studied, and physical mechanisms leading to temperature defect and flow reversal are presented. The numerical results were checked by testing stability and convergence, and they were also compared with experimental data reported in the literature.

CHAPTER I
INTRODUCTION

Natural convection problems are usually divided into two categories. external problems, such as flow and heat transfer from a heated rod or plate to a fluid at rest, and internal problems, such as flow and heat transfer between parallel plates or in a fluid-filled enclosure. Much of the earlier work on convection studies has been concentrated on tha external problems. The internal problems have received attention more recently and it is due to the fact that the convection in an enclosed space is complicated.

For an external problem of natural convection from a heated rod ar plate to a fluid at rest, the Prandtl boundary layer theory can be used to simplify its governing equations. The ambient condition is also unaffected by the heat transfer. For an internal problem of natural convection in a confined space, however, a core region is surrounded by the boundary-layer regions near the walls, and the coupling of these two regions leads to a great complexity in heat transfer analysis.

The internal convection problems have extensive applications in geophysics and engineering. For example, geophysicists are interested in studying the fluid motion induced by density gradient in a cavity. Solar energy specialists are interested in suppressing the natural-convection heat loss in solar collectors. With the

recent miniaturization of electronic equipment, electrical engineers also became interested in the convection problems. Certainly, these convection problems remain a major area of research in heat transfer engineers, and the recently developed numerical methods enable them to model complicated convection problems more realistically, as a result, there is an outburst of convection research as reported in the literature (a review follows in the next chapter).

It is the purpose of this dissertation to study numerically the natural convection of water in a stratified enclosure. The numerical solution is applied to compare two alternatives in the design of solar energy storage tanks, one placing insulation on the outside surface of the tank (a common practice), and the other placing the insulation over the inside of the tank wall (a new idea). Since it is important to maintain stratification in the storage tank in order to raise the overall efficiency of a solar energy system, it will be shown that significant improvement in stratification can be realized by placing the insulation over the interior of the tank wall. It is hoped that the insight gained from this research will be useful in the future design of solar energy storage systems.

CHAPTER II
LITERATURE REVIEW

The internal convection problems have been extensively reviewed by Ostrech [1] in 1972 and by Catton [2] in 1978. Since the present dissertation will deal with a study of unsteady natural convection in enclosures with stratified medium, and the study is related to the analysis of storage of thermal energy for solar energy applications, the convection review that is to follow will address these two areas of research as documented in the literature.

2.1 Natural Convection in Enclosures

For natural convection in rectangular and cylindrical enclosures bounded by vertical side walls (i.e., vertical enclosures) either heated or cooled, two types of problems usually arise and are reviewed here. The first type of problem deals with side walls imposed with different temperatures, commonly known as differentially heated conditions, see Figure 2.1(a). The second type of problem has these walls imposed with symmetrical conditions, either constant temperature or constant heat flux, for ease of reference later to this second problem, these will be called symmetrically heated conditions, see an example shown in Figure 2.1(b). The top and bottom boundaries for both problems are usually insulated.

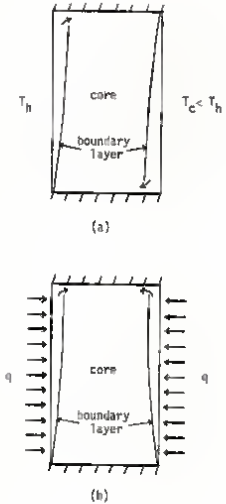

Figure 2.1 Natural convection in enclosures

2.1.1 Differentially Heated Conditions

In 1954, Batchelar [3] studied natural convection in gas inside a rectangular enclosure imposed with isothermal side walls and either perfectly conducting or insulating top and bottom surfaces. From the analytical results obtained, he reasoned that several flow regimes occur inside the enclosure depending on the aspect ratio of the enclosure and the Rayleigh number. Eckert and Carlson [4] tested with enclosures made up of isothermal side walls at temperature differences ranging from 5° to 90°C. They were able to define conduction, transition, and boundary-layer regimes as functions of the Grashof number and the aspect ratio. The enclosed core region, however, was not isothermal as predicted by Batchelar, but stratified in that the temperature was uniform horizontally but increased in a vertical direction. Elder [5] made a study of natural convection in water in a vertical slot with aspect ratios ranging from 1 to 80 and obtained basically the same results as Eckert and Carlson. An analytical study by Gill [6] provided further proof of Eckert and Carlson's observations.

The convection research carried out so far has established that the basic flows inside an enclosure consist of two boundary layers near the heated or cooled walls, and the fluid in the enclosed core region is temperature stratified, see Figure 2.1(a). Schinkel et al, [7] studied the effect of core stratification on natural convection and showed that the stratification in the core region had an effect of decreasing buoyancy force and producing secondary flows in the fluid. Bahn et al, [8] were able to show that the boundary-layer

flows near the side walls were actually responsible for the heat transfer across the enclosure. For the boundary conditions illustrated in Figure 2.1(a), the fluid moves up near the heated wall, drifts across the top of the enclosure, and then descends along the cooled wall at the other side.

The construction of the enclosure wall also has an affect on the convective flow in the enclosure. Gdalevich et al. [9] studied numerically the heat transfer in a vertically bounded air space, only one of the side walls had a finite thickness and the thermal conductivity of this wall was treated as a variable, the outside surface of this wall being imposed with an isothermal condition. The other side wall was also isothermal but at a different temperature. As expected, an increase of the thermal resistance in the thick wall leads to a drop in the intensity of the convective motion in the enclosure.

In the event that the top and bottom end walls of the enclosure are not adiabatic, then the constructions of these walls also have a bearing on the heat transfer. Meyer et al. [10] have shown that the convective coefficients for enclosures fitted with adiabatic end walls are substantially higher than those with conducting walls. A study by Elsherbiny et al. [11] gave qualitative results for wall conduction, radiation, and convection interactions; they also proposed a list of parameters that must be specified when reporting data for enclosures bounded by conducting end walls. More recently, Kim and Viskanta [12] reported both experimental and numerical results on the effects of wall conductance on natural convection in a

rectangular cavity. They tested three different heating and cooling arrangements in which the external walls of the cavity was heated from either the side, the top or the bottom, while at the same time, the heat was removed from the opposing wall of the cavity. They showed that the heat conduction in the connecting (unheated) walls had an effect of either stabilizing or destabilizing the fluid motion in the cavity.

Most of the convection problems studied in the literature deal with two-dimensional systems in which the enclosure is treated as infinitely long in the third dimension; in reality, however, the enclosure is of finite length, and the third dimension is expected to have an effect on the fluid motion. Morrison and Tran [13] used a laser Doppler anemometer to measure velocity profiles and showed that three-dimensional flow was induced by the heat loss from the vertical end walls in the third dimension. Horizontal velocity component normal to the end walls is small as compared with the vertical component when these walls are well insulated. However, when they are not, as these found in many heat transfer experiments, a strong three-dimensional motion is detected. Mallinson and Vahl Davis [14] used a numerical method to show that the end effect was mainly confined to the vicinity of the end walls for air or high Prandtl fluids. A two-dimensional model is considered adequate for convection analysis as long as the Rayleigh and Prandtl numbers are large and the cavity is long in the third dimension.

2.1.2 Symmetrically Heated Conditions

When the enclosure is symmetrically heated or cooled from the side walls, top and bottom surfaces being insulated as shown in Figure 2.1(b), the core region is again surrounded by the boundary regions. Schwind and Vliet [15] used both the Schlieren and shadowgraph techniques to study the natural convection and stratification of water in a vessel with heated side walls and a free top water surface. The fluid motion leading to the formation of stratified layers was studied in great detail, and a reverse shear flow was found near the boundary layers in the presence of a large adverse temperature gradient in the core region. Evans et al [16] tested with liquids in a partially filled cylindrical container with uniform heat flux applied on the side wall. They developed an analytical model for studying the fluid flow in the container. To simplify their analysis, they divided the container into three regions: a thin boundary layer near the side wall, a mixing region at the top where the boundary layer discharges and mixes with the upper core fluid, and a main core region which gradually diminishes in height because of the mixing of the fluid from above. Numerical results computed with this model were found in close agreement with experiment. Evans' work was further extended by Hess and Miller [17] to cover heat transfer in the container wall. A thermocline-type cylindrical enclosure with its side wall imposed with an isothermal condition was solved with an integral method, and the results were found in good agreement with the finite-difference solution and the

experimental data which Hess and Miller obtained in an earlier study [18].

Transient natural convection in a cavity has also been an area of interest. Barakat and Clark [19] made a numerical study of natural convection in a partially filled liquid container whose walls were subjected to arbitrary time- and space-dependent temperature variations. An explicit finite-difference technique was developed for the solution of this problem. A method of stability analysis suitable for solving partial differential equations with variable coefficients was also included in their paper. An interesting study was made by Sakurai and Matsuda [20] that involved Boussinesq fluid in a circular cylinder. The top of this cylinder was at a higher temperature then the bottom so the temperature distribution in the fluid was thermally stable. The side wall was made up of a good thermal conductor with small time constant. At a certain moment, the top and bottom temperatures of this cylinder were changed suddenly by an equal amount but in opposite sign, and the convection in the cylinder was studied as it responded to the temperature change in the side wall. They were able to show analytically that a meridional circulation in the core region was induced by the boundary-layer flow near the side wall. This circulation redistributed the fluid to the extent that a new state of stratification took place in the core region. Sakurai and Matsuda's work was further extended by Jischke and Doty [21] who studied the transient flow in an arbitrarily-shaped container, completely filled with fluid. The temperature of the container wall was impulsively changed and it was found that the

invisid interior region heated up by a convective process that was driven by suction induced by the boundary layer. The inviscid, adiabatic interior, however, responded to a horizontal average temperature perturbation of the wall because the boundary layer smeared out the circumferential temperature variation. The interior thus, in effect, responded to an isothermal boundary in each horizontal plane. Four examples were provided in their paper for substantiation of their theory.

Hess and Miller [18] used a laser Doppler velocimeter to measure velocity field inside a thermocline-type cylindrical enclosure. Both the axial and radial components of the velocity were measured and found to have a magnitude ranging from 0.01 to 0.45 cm/s. Good agreement was also found with a numerical solution.

2.2 Energy Storage in a Thermocline or a Stratified Medium

Storage of solar energy in a stratified medium is always desirable in air-heating systems and domestic hot water systems [22]. In practice, the heated medium from a solar collector enters the top of a stratified storage tank, and the medium leaving the bottom of the tank enters the collector at a lower temperature. This arrangement permits the collector to be operated at a constant, high efficiency, which is important to the performance of the total system.

Numerous models have been developed to simulate the fluid flow in a stratified tank. Close [23] developed an analytical model in which the tank was divided into several well-mixed sections. By postulating that the incoming hot fluid would seek a section for home that has the same density level as the incoming fluid, he was able to

develop partial differential equations for energy balance in each section. A three-section model was found adequate for simulating the performance of a water heating system [24]. Close's analytical model is considered useful when the fluid velocity entering the storage tank is small. When this velocity is large, however, turbulent mixing effect must be accounted for. Wu and Han [25] considered viscous entrainment in their mathematical model. A set of partial differential equations was developed by them and solved with an implicit finite-difference method.

Cabelli [26] developed a two-dimensional model for studying the fluid flow and temperature distribution in a storage tank. Both charging and discharging situations were modelled numerically and it was found that a one-dimensional analysis, such as that developed by Close, should provide reasonable accuracy in predicting the temperature profiles in a tank if the hot medium enters at the top of the tank. Sha and Lin [27] were able to develop a three-dimensional model for analyzing the flow stratification in a thermocline storage tank. They developed a computer program (COMMIX-SA) for analysis and the model was shown to give good prediction of the fluid flow and temperature distribution in the tank during a demand mode.

The benefit of thermal stratification has also been documented in the literature. Sharp and Loehrke [28] studied numerically the potential benefits of thermal stratification in a solar space heating application. They compared the performance of a system with stratified storage to that of a similar system with well-mixed storage and found that the benefit due to stratification, as measured

by the increase in the fraction of the total heating load supplied by solar energy, ranged from 5 to 15%. The benefit of thermal stratification was also verified by Veltkamp [29] using both experiment and numerical modelling. For low temperature applications under a low flow-rate condition, a stratified storage was able to enhance the total system efficiency by 10% or more. They also noted that, in order to numerically model the storage tank with accuracy, it was necessary to divide the tank into 20 sections at least, a proposal in sharp contradiction to the division recommendation made by Gutierrez et al. [24] in an earlier study. Cole and Bellinger [30] proposed a new strategy for controlling stratification that enabled lowering of the average collector operating temperature by as much as 20°C. This reduction of collector temperature also resulted in an improvement in the total system performance up to 20%.

The decay of thermal stratification has been studied in the literature. Viskanta and Hale [31] studied unsteady natural convection in a thermally stratified tank driven by heat losses through tank walls. A two-dimensional model was used in their analysis and the results indicated that the natural convection was not confined to the vicinity of the walls but spread out to fill up the entire tank. To reduce the degradation of the thermocline and unwanted heat transfer between the hot and cold regions, the tank should be well insulated. Jaluria and Gupta [32] developed a one-dimensional model to analyze the decay of thermal stratification in a water body under a static condition. For the plexiglass container used in their analysis, they noted that the cooling process in the

water depended strongly on its initial condition. A stratified water body was able to curb mixing, and the energy transfer inside the stratified region was mainly a result of thermal diffusion. Grass [33] made a similar study of decay of stratification in a thermocline system. He determined the relative importance of each of the five heat loss mechanisms present in the system that include (1) heat loss to ambient, (2) convective motion induced by heat transfer from the hot layer to the cold layer via the highly conductive tank wall, (3) mixing during charging and discharging, (4) thermosiphoning loops in the inlet and outlet manifolds, and (5) thermal diffusion from the hot layer to the cold layer. Strategies to cut down on these losses were also proposed in his paper.

Lavan and Thompson [34] studied experimentally the thermal stratification in a hot-water storage tank under a high extraction-rate condition. Parameters studied included the aspect ratio of the tank, the water inlet-outlet temperature difference, the inlet and exit port configuration, and the water mass flow rate. Sherman et al. [35] made an experimental study of the effect of wall conductance on the temperature relaxation time of a stratified tank under a static condition. From the five sets of data they collected, they were able to show that conduction along the tank wall could cause decay of thermal stratification to a significant extent. Mlifer [36] showed that the natural convection generated at the fluid/wall interface of a stratified tank increased for larger Rayleigh numbers, but decreased for larger aspect ratios of the tank. This natural convection also increased proportionally to the square root of the

thickness of the tank wall. Chaney et al. [37] suggested the idea of insulating the interior surface of the storage-tank wall in order to cut down on the heat leak, however, they provided no verification of the usefulness of this idea.

CHAPTER III
MATHEMATICAL FORMULATION

The system under investigation is shown schematically in Figure 3.1. A cylindrical tank filled with water, with top and bottom surfaces insulated, is chosen for analysis. The water temperature changes with time due to heat loss through the tank wall. In order to compare the performances of the tank with different designs of the wall, the insulation on the wall is placed either on the outside or on the inside of the wall. An uninsulated tank is also tested for control. The entire system analyzed is divided into three regions. the water occupies the space $R_i > r > 0$, the wall/insulation is in the region $R_o > r > R_i$, and the air is in $r > R_o$.

The water is assumed initially stratified as shown by the isotherms plotted in the figure. The water bodies in the top and bottom sections of the tank are isothermal but at different (dimensionless) temperatures. In the middle section, the water temperature is linearly stratified as shown by those horizontal lines drawn. The initial temperature of the tank wall is assumed unity throughout, a condition necessary to provide perturbation in water to initiate convection.

For the problem under investigation, the water is considered viscous and having constant properties (except density), the natural convection is laminar. In the tank wall, the thermal diffusivity is

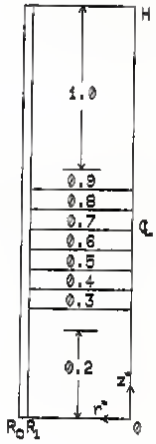

Figure 3.1 Coordinate system and initial temperature distribution

treated as constant. The temperature distributions in the water and wall are to be investigated, and they are found by solving governing equations in these two regions.

3.1 Governing Equations and Conditions for Natural Convection in Water

The conservation of mass, momentum, and energy in water may be expressed in three equations as follows [38]:

Continuity Equation.

$$\frac{D\rho}{D\tau} + \rho\nabla\cdot\vec{V} = 0 \tag{3.1}$$

Momentum Equation:

$$\rho\frac{D\vec{V}}{D\tau} = \vec{F} - \nabla P + \mu\nabla^2\vec{V} + \frac{\mu}{3}\nabla(\nabla\cdot\vec{V}) \tag{3.2}$$

Energy Equation

$$\rho C_p\frac{DT}{D\tau} = \nabla\cdot k\nabla T + \beta T\frac{DP}{D\tau} + \mu\Phi + Q' \tag{3.3}$$

With the assumptions made earlier, the pressure, dissipation, and source terms in the energy equation may be neglected. In the momentum equation,

$$\vec{F} - \nabla P = (\rho - \rho_a)\vec{g} - \nabla P_d \tag{3.4}$$

Boussinesq approximations are used to relate the density difference to temperature difference as

$$\rho - \rho_a = \rho\beta(T_a - T) \tag{3.5}$$

The density differential term in the continuity equation may be dropped, thus giving a new set of simplified equations:

$$\nabla\cdot\bar{V} = 0 \tag{3.6}$$

$$\rho\frac{D\bar{V}}{Dt} = \rho\bar{g}\beta(T_a - T) - \nabla p_d + \mu\nabla^2\bar{V} \tag{3.7}$$

$$\rho C_p\frac{DT}{Dt} = k\nabla^2 T \tag{3.8}$$

As expected, the momentum and energy equations are coupled through the temperature terms in these equations.

Equations (3.6) through (3.8) are specialized to the case of a two-dimensional cylindrical system of interest in this study. A set of four equations is written as follows:

Continuity Equation

$$\frac{\partial V_r}{\partial r} + \frac{1}{r}V_r + \frac{\partial V_z}{\partial z} = 0 \tag{3.9}$$

Momentum Equation in r Direction:

$$\frac{\partial V_r}{\partial t} + V_r\frac{\partial V_r}{\partial r} + V_z\frac{\partial V_r}{\partial z} = -\frac{1}{\rho}\frac{\partial p_d}{\partial r} + \nu\left(\frac{1}{r}\frac{\partial}{\partial r}\left(r\frac{\partial V_r}{\partial r}\right)\right.$$

$$- \frac{V_r}{r^2} + \frac{\partial^2 V_r}{\partial z^2}] \qquad (3.10)$$

Momentum Equation in z Direction.

$$\frac{\partial V_z}{\partial t} + V_r \frac{\partial V_z}{\partial r} + V_z \frac{\partial V_z}{\partial z} = - \frac{1}{\rho} \frac{\partial P_d}{\partial z} + \nu[\frac{1}{r} \frac{\partial}{\partial r}(r \frac{\partial V_z}{\partial r})$$

$$+ \frac{\partial^2 V_z}{\partial z^2}] + g\beta(T - T_a) \qquad (3.11)$$

Energy Equation

$$\frac{\partial T}{\partial t} + V_r \frac{\partial T}{\partial r} + V_z \frac{\partial T}{\partial z} = \alpha(\frac{\partial^2 T}{\partial r^2} + \frac{1}{r} \frac{\partial T}{\partial r} + \frac{\partial^2 T}{\partial z^2}) \qquad (3.12)$$

Eliminating pressure terms in the two momentum equations given above and relating the stream function, ψ, and the velocity components

$$V_r = - \frac{1}{r} \frac{\partial \psi}{\partial z}$$

$$V_z = \frac{1}{r} \frac{\partial \psi}{\partial r} \qquad (3.13)$$

and further introducing the vorticity relation

$$\omega = \frac{\partial V_r}{\partial z} - \frac{\partial V_z}{\partial r} \qquad (3.14)$$

give the vorticity transport equation

$$\frac{\partial \omega}{\partial t} + \frac{\partial}{\partial r}(V_r \omega) + \frac{\partial}{\partial z}(V_z \omega) = -g\beta \frac{\partial T}{\partial r} + \nu\left[\frac{\partial^2 \omega}{\partial z^2} + \frac{\partial}{\partial r}\left(\frac{1}{r}\frac{\partial (r\omega)}{\partial r}\right)\right] \tag{3.15}$$

The energy equation may also be recast as

$$\frac{\partial T}{\partial t} + \frac{1}{r}\frac{\partial}{\partial r}(rV_r T) + \frac{\partial}{\partial z}(V_z T) = \alpha\left[\frac{\partial^2 T}{\partial z^2} + \frac{1}{r}\frac{\partial}{\partial r}\left(r\frac{\partial T}{\partial r}\right)\right] \tag{3.16}$$

It is common practice in the fluid flow and heat transfer analysis to introduce dimensionless groups

$$\begin{aligned} r_f^* &= \frac{r}{R_i} & z^* &= \frac{z}{H} \\ u^* &= \frac{V_z R_i}{\alpha_f} & v^* &= \frac{V_r R_i}{\alpha_f} \\ t^* &= \frac{\alpha_f t}{R_i H} & T_f^* &= \frac{T_f - T_\infty}{T_{s,0} - T_\infty} \\ \omega^* &= \frac{\omega R_i H}{\alpha_f} & \psi^* &= \frac{\psi}{\alpha_f R_i} \end{aligned} \tag{3.17}$$

so that the number of variables to be considered in the analysis may be reduced. For the sake of convenience in expressions, the asterisks in these dimensionless quantities are dropped. Then, the vorticity transport equation, the stream function equation, the velocity equations, and the energy equation may be expressed as follows:

Vorticity Transport Equation.

$$\frac{\partial \omega}{\partial t} + \frac{\partial}{\partial r_f}(v\omega) + \frac{\partial}{\partial z}(u\omega) = Pr[A \frac{\partial}{\partial r_f}(\frac{1}{r_f}\frac{\partial}{\partial r_f}(r_f\omega)) + \frac{1}{A}\frac{\partial^2 \omega}{\partial z^2}]$$

$$- \frac{RaPr}{A}\frac{\partial T_f}{\partial r_f} \qquad (3.18)$$

Stream Function Equation:

$$\frac{1}{Ar_f}\frac{\partial}{\partial z}(\frac{\partial \psi}{\partial z}) + A\frac{\partial}{\partial r_f}(\frac{1}{r_f}\frac{\partial \psi}{\partial r_f}) = -\omega \qquad (3.19)$$

Velocity Equations.

$$u = \frac{1}{r_f}\frac{\partial \psi}{\partial r_f} \qquad (3.20)$$

$$v = -\frac{1}{r_f}\frac{\partial \psi}{\partial z} \qquad (3.21)$$

Energy Equation:

$$\frac{\partial T_f}{\partial t} + \frac{1}{r_f}\frac{\partial}{\partial r_f}(r_f v T_f) + \frac{\partial}{\partial z}(uT_f) = A[\frac{1}{r_f}\frac{\partial}{\partial r_f}(r_f \frac{\partial T_f}{\partial r_f})] + \frac{1}{A}\frac{\partial^2 T_f}{\partial z^2} \qquad (3.22)$$

The initial and boundary conditions for water may be summarized as

$$T_f(r_f,z,0) = T_{f,0}(r_f,z)$$

$$z = 0 , \quad v = 0 , \quad \frac{\partial \psi}{\partial z} = 0 , \quad \frac{\partial T_f}{\partial z} = 0 ,$$

$$z = 1 , \quad \psi = 0 , \quad \frac{\partial \psi}{\partial z} = 0 , \quad \frac{\partial T_f}{\partial z} = 0 , \tag{3.23}$$

$$r_f = 0 , \quad \psi = 0 , \quad u = 0 , \quad \frac{\partial T_f}{\partial r_f} = 0 ,$$

$$r_f = 1 , \quad \psi = 0 , \quad \frac{\partial \psi}{\partial r_f} = 0 , \quad T_f(1,z,t) = T_i(z,t)$$

Notice that there are five unknowns (ω, ψ, u, v, and T_f) in the governing equations (3.18) through (3.22), and there are five equations here to solve them.

3.2 Governing Equations and Conditions for Heat Conduction in Wall

The energy equation in the tank wall is the heat conduction equation

$$\frac{\partial T}{\partial t} = \frac{1}{r} \frac{\partial}{\partial r}\left[r \frac{\partial (\alpha T)}{\partial r}\right] + \frac{\partial^2 (\alpha T)}{\partial z^2} \tag{3.24}$$

in which the diffusivity, α, has been placed after the partial differential operators in order to allow its use in the analysis of heat conduction in walls with or without insulation.

The following dimensionless groups are introduced for the wall

$$r_s^* = \frac{r - R_i}{R_o - R_i} = \frac{r - R_i}{\delta} , \qquad z^* = \frac{z}{H}$$

(3.25)

$$t^* = \frac{\alpha_f t}{R_f^2} \qquad , \qquad T_s^* = \frac{T_s - T_\infty}{T_{s,0} - T_\infty}$$

and once again, the asterisks are dropped and equation (3.24) is recast as

$$\frac{\partial T_s}{\partial t} = B \frac{\partial^2(rT_s)}{\partial r_s^2} + \frac{\delta B}{R_f + \delta r_s} \frac{\partial(rT_s)}{\partial r_s} + \frac{1}{\lambda} \frac{\partial^2(rT_s)}{\partial z^2} \tag{3.26}$$

where

$$\alpha = \frac{\alpha_s}{\alpha_f}$$

and

$$B = \frac{\delta R_f}{\delta^2}$$

Initial and boundary conditions for the wall are given by the relations

$$\begin{aligned}
&T_s(r_s,z,0) = T_s(r_s,z) \\
&z = 0 \,, \quad \frac{\partial T_s}{\partial z} = 0 \,, \\
&z = 1 \,, \quad \frac{\partial T_s}{\partial z} = 0 \,, \\
&r_s = 0 \,, \quad T_s(0,z,\tau) = T_f(z,t)
\end{aligned} \tag{3.27}$$

$$r_s = 1 , \qquad \frac{\partial T_s}{\partial r_s} + \frac{hs}{k_s} T_s = 0$$

Notice that the dimensionless radius in the wall has been redefined with reference to the wall itself, such a change permits the conditions of the wall to be expressed more compactly as those given above.

For the problem given, only the ambient air temperature, T_∞, is fixed; the water temperature is constantly changing with time due to heat loss through the tank wall. In fact, the wall temperature also changes, but the heat fluxes and temperatures at the wall/water interface remain continuous at any instant of time. This situation presents a conjugate heat transfer problem in that conduction in the wall and convection in the water must be considered simultaneously, with proper matching of conditions at the interface. This problem can only be solved numerically as will be shown in the next two chapters.

CHAPTER IV
METHODS OF SOLUTION

Several problems are encountered and must be resolved before the governing equations given in Chapter III can be solved numerically. Also, these governing (differential) equations must be discretized and appropriate numerical methods must be chosen to solve them. All these must be done at the early stage of the solution of the problem.

4.I Special Treatment in the Solution

Special treatment is needed to resolve several problems described in this section.

4.I.1 Computation of Heat Loss from Wall to the Ambient Air

It must be noted that, in the formulation of the governing equations given in the preceding chapter, only those in the storage medium (water) and the tank wall have been given. The external convection from the wall to the ambient air has not been considered as a separate region but accounted for in the boundary conditions for the wall. Certainly, it is possible to consider the external convection as a separate problem and solve it together with the wall and water problems; however, such a decision would require matching of extra conditions at the wall/air interface in addition to the solution of the heat transfer in the air, an exceedingly laborious task even for a computer to handle. The present treatment of the

external convection by means of use of proper boundary conditions for the wall is therefore preferred.

In the search of empirical equations for estimating wall heat loss, attention must be given to the fact that the wall is nonisothermal. In reality, the outside wall temperature is the result of the wall heat flux, which is, in turn, related to the temperature of the wall itself. It is thus desirable to find empirical relations that permit a simultaneous determination of the temperature and heat flux in the wall.

The external convection from a nonisothermal, vertical wall has been a subject of numerous studies [38-43]. Of these references cited, Sparrow and Gregg [38] and Karvinen's analyses [40] are chosen for comparison. Sparrow and Gregg used a similarity analysis to evaluate the Nusselt number for natural convection from a vertical wall on which the temperature distribution followed a power-law relationship

$$T_s - T_\infty = Nz^m \tag{4.1}$$

Sparrow and Gregg presented their results graphically, a fit of their curves using a cubic polynomial yields the relation

$$\frac{Nu_z}{\left(\frac{Gr_z}{4}\right)^{\frac{1}{4}}} = 0.02568\, m^3 - 0.135\, m^2 + 0.3623\, m + 0.5018 \tag{4.2}$$

Notice that, although the temperature of the wall varies with N in

equation (4.1), the Nusselt-number equation correlated above is independent of it.

Karvinen used the approximate solution methods of Saithby and Hollands [44] and developed a relation between the wall heat flux and wall temperature distribution

$$q(z) = Ck_m\left(\frac{g\beta Pr}{\nu^2}\right)^{\frac{1}{4}} \Delta T_s^{\frac{5}{3}} \left[\int_0^z \Delta T_s^{\frac{5}{3}}\, dz\right]^{-\frac{1}{4}} \tag{4.3}$$

where Prandtl number, Pr, is greater than 0.6, ΔT_s stands for a temperature difference, $T_s - T_\infty$. The constant C is related to the Prandtl number as follows:

$$C = \frac{0.503}{\left[1 + \left(\frac{0.492}{Pr}\right)^{\frac{9}{16}}\right]^{\frac{4}{9}}} \tag{4.4}$$

By modelling the temperature variation on the wall as a series of linear functions, Karvinen was able to integrate equation (4.3) to give

$$q(z) = Ck_m\left(\frac{g\beta Pr}{\nu^2}\right)^{\frac{1}{4}} \Delta T_s^{\frac{5}{3}} \left\{\sum_{j=1}^{n} \frac{3}{8D_j}\left(\Delta T_{s,j}^{\frac{8}{3}} - \Delta T_{s,j-1}^{\frac{8}{3}}\right)\right\}^{-\frac{1}{4}} \tag{4.5}$$

where

$$D_j = \frac{\Delta T_{s,j} - \Delta T_{s,j-1}}{z_j - z_{j-1}}$$

Equation (4.5) may be used together with Newton's cooling law to evaluate the local convective coefficient.

For a power-law temperature variation given as equation (4.1), equation (4.3) may be integrated to give

$$\frac{Nu_z}{\left(\frac{Gr_z}{4}\right)^{\frac{1}{4}}} = 0.4586\left(\frac{3}{5m+3}\right)^{-\frac{1}{4}} \tag{4.6}$$

This equation may be used to test the accuracy of the approximate solution by Karvinen. Numerical results are obtained for both solution methods in which the Prandtl number is taken to be 0.7 (air). As is shown in Table 4.1, the error in the $Nu_z/(Gr_z/4)^{1/4}$ values computed with the approximate solution increases with m. For all the m values tested, the approximate solution always gives a lower estimation of the Nusselt number.

In selecting a prediction method from the two approaches compared above, consideration was given to the fact that (1) it is difficult to fit the wall temperature using the temperature relation given by equation (4.1), and (2) even for situations where the wall temperature can be fitted by this equation, the exponent m for z is usually small (< 0.2). For these reasons, Karvinen's equation (4.5) is preferred. A point should be noted, however. The fact that his equation was derived on the basis of heat transfer from a flat wall does not affect its use in the present analysis because the storage

Table 4.1 Comparison of exact solution and approximate solution for heat loss calculation

m	$Nu_z/(Gr_z/4)^{1/4}$ exact (eq. (4.2))	$Nu_z/(Gr_z/4)^{1/4}$ approximate (eq. (4.6))	error %
0*	0.5018	0.4986	0.64
0.1	0.5357	0.5182	3.27
0.2	0.5671	0.5356	5.52
0.3	0.5960	0.5518	7.42
0.4	0.6228	0.5665	9.04
0.5	0.6474	0.5802	10.38
0.6	0.6701	0.5929	11.52
0.7	0.6911	0.6049	12.47
0.8	0.7104	0.6162	13.26
0.9	0.7282	0.6269	13.91
1.0	0.7448	0.6372	14.45

* isothermal condition

tank under investigation has a small curvature, according to a numerical study made by Cebeci [45].

4.1.2 Matching of Conditions at Wall/Water and Wall/Insulation Interfaces

For the conjugate heat transfer problem solved in this work, both the heat fluxes and the temperatures must be continuous at all interfaces. As has been mentioned before, the heat flux is related to the temperature, neither of these two quantities, therefore, being known a priori.

The interface conditions may be matched by different methods as reported in the literature, see references in the literature [36,46,47, for example]. The method used in this work to match wall/water interface conditions is derived on the basis of the use of continuity of temperature

$$T_s(0,z,t) = T_f(1,z,t) = T_f(z,t) \tag{4.7}$$

and heat flux

$$-k_s \frac{\partial T_s}{\partial r_s}\bigg|_{r_s=0} = -k_f \frac{\partial T_f}{R_i \partial r_f}\bigg|_{r_f=1} \tag{4.8}$$

By writing equation (4.8) in a finite-difference form and incorporating it with (4.7), it is possible to write the interface temperature as

$$T_i = \frac{T_{f,-1} + \frac{k_s R_i \Delta r_f}{k_f \Delta r_s} T_{s,-1}}{1 + \frac{k_s R_i \Delta r_f}{k_f \Delta r_s}} \tag{4.9}$$

where $T_{f,-1}$ and $T_{s,-1}$ represent temperatures one grid point away from the interface in the fluid and the solid region, respectively, Δr_f and Δr_s refer to mesh lengths in these regions. In the numerical work to be presented later, this interface temperature, T_i, is used as a common boundary condition for both wall and water regions, and the wall and water energy equations are solved simultaneously. Heat fluxes across the interface are then computed, and if they fail to agree, the newly computed temperatures are used to recalculate interface temperature using equation (4.9). This procedure is repeated until all heat fluxes match at the interface.

For the interface between the wall and the insulation, a different method is used. By considering the wall and the insulation as a single region in the numerical computation, it is possible to use Patankar's control volume approach [46] to lay out the grid points as shown in Figure 4.1. There is no grid point right at the interface, the difference in material may be accounted for by introducing an interface diffusivity

$$\alpha_i = \frac{k_i}{\rho_i c_{p,i}} \tag{4.10}$$

in which k_i denotes a harmonic mean conductivity [46]

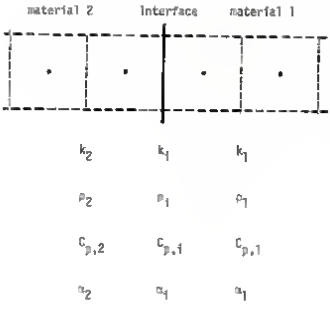

Figure 4.1 Interface properties

$$k_i = \frac{2k_1k_2}{k_1 + k_2} \tag{4.11}$$

and $a_i C_{p,i}$ denotes an arithmatic mean heat capacitance

$$a_i C_{p,i} = \frac{a_1 C_{p,1} + a_2 C_{p,2}}{2} \tag{4.12}$$

With the use of these quantities, the continuity of heat fluxes at the interface may be satisfied implicitly.

4.1.3 Kinematically Consistent Velocity Fields

It has been well established that finite difference approximations for conservation of mass, vorticity, and energy are relatively easy to derive for a system in Cartesian coordinates. In cylindrical coordinates, however, they are more difficult to derive because the transport velocities (normal velocity components on grid volumes), if improperly expressed in terms of stream functions, may lead to a situation in which the conservation of volume flow is not satisfied on the grid volume.

Parmenter and Torrance [48] derived kinematically consistent velocities for use in cylindrical coordinates. The derivations that follow are credited to their work but modified slightly in order to account for the nonuniform grid system used in the present study.

It is imperative that kinematically consistent velocities must satisfy the circulation theorem both locally and globally

$$\int_S \omega dS = \int_\gamma \bar{V} \cdot d\bar{\gamma} \tag{4.13}$$

In this equation s and l represent respectively the area and the perimeter of the region of integration. In a dimensionless form, equation (4.13) can be expressed as

$$\int_s \omega dz dr = A \int \omega dz + \frac{1}{A} \int v dr \tag{4.14}$$

where A is aspect ratio, H/R_1. Approximation of the integrals in the above equation leads to the following expression for the area-averaged vorticity in the grid volume

$$\omega_{i,j} = \frac{A(u^t_{i,j-1} - u^t_{i,j})\nabla z_i + \frac{1}{A}(v^t_{i,j} - v^t_{i-1,j})\nabla r_j}{\nabla z_i \nabla r_j} \tag{4.15}$$

where $\nabla z_i = (z_{i+1} - z_{i-1})/2$ = dimension of grid volume in z direction

$\nabla r_j = (r_{j+1} - r_{j-1})/2$ = dimension of grid volume in r direction

Consider an interior grid point in a nonuniform grid system shown in Figure 4.2. Since the faces of the grid volume are located midway between the mesh points in each direction, approximations for tangential velocities in terms of stream function may be obtained from equations (3.20) and (3.21) as

$$u^t_{i,j} = \frac{\psi_{i,j+1} - \psi_{i,j}}{r_{j+\frac{1}{2}} \Delta r_j}$$

$$v^t_{i,j} = -\frac{1}{r_j} \frac{\psi_{i+1,j} - \psi_{i,j}}{\Delta z_i} \tag{4.16}$$

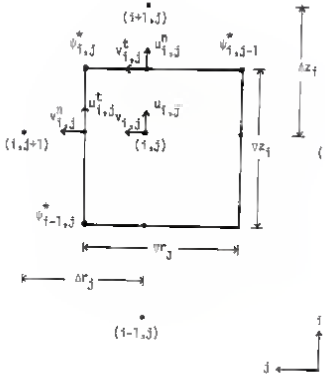

Figure 4.2 Notations for an interior grid volume in a nonuniform cylindrical grid system

Velocities at grid points may then be expressed in terms of these velocities as

$$u_{i,j} = \frac{u^t_{i,j} + u^t_{i,j-1}}{2}$$

$$v_{i,j} = \frac{v^t_{i,j} + v^t_{i-1,j}}{2} \qquad (4.17)$$

Upon substitution of equation (4.16), equetion (4.15) becomes

$$\omega_{i,j} = -\frac{A}{\forall r_j}\left(\frac{1}{r_{j+\frac{1}{2}}}\frac{\psi_{i,j+1} - \psi_{i,j}}{r_{j+1} - r_j} - \frac{1}{r_{j-\frac{1}{2}}}\frac{\psi_{i,j} - \psi_{i,j-1}}{r_j - r_{j-1}}\right)$$

$$- \frac{1}{A\forall z_i}\left(\frac{1}{r_j}\frac{\psi_{i+1,j} - \psi_{i,j}}{z_{i+1} - z_i} - \frac{1}{r_j}\frac{\psi_{i,j} - \psi_{i-1,j}}{z_i - z_{i-1}}\right) \qquad (4.18)$$

This is the finite-difference form of the stream function equation (3.19). Here the circulation theorem has been used for derivation, Taylor's series may be used to derive the same equation, as is not unexpected.

For an incompressible medium, the normal velocity components (transport velocities) must be defined with the following relations

$$u^n_{i,j} = \frac{1}{\forall r_j}\frac{\psi^*_{i,j} - \psi^*_{i,j-1}}{}$$

$$v^n_{i,j} = -\frac{1}{r_{j+\frac{1}{2}}}\frac{\psi^*_{i,j} - \psi^*_{i-1,j}}{\forall z_i} \qquad (4.19)$$

so that the volume flow is conserved on the grid volume. The asterisked stream functions refer to the stream functions at the corners of the grid volume, see Figure 4.2. These corner stream functions are related to the stream functions at grid points by the relation

$$\psi^*_{i,j} = \alpha_j\left(\frac{\psi_{i,j} + \psi_{i+1,j}}{2}\right) + \beta_j\left(\frac{\psi_{i,j+1} + \psi_{i+1,j+1}}{2}\right) \tag{4.20}$$

In order for the mass flow to satisfy the conservation principle, the weighting functions, α_j and β_j, must take on those values listed in Table 4.2.

Combining equations (4.19) and (4.20) gives expressions for the transport velocities as

$$u^0_{i,j} = \frac{1}{r_j w_j}\left[\alpha_j\left(\frac{\psi_{i,j} + \psi_{i+1,j}}{2}\right) + \beta_j\left(\frac{\psi_{i,j+1} + \psi_{i+1,j+1}}{2}\right)\right.$$
$$\left. - \alpha_{j-1}\left(\frac{\psi_{i,j-1} + \psi_{i+1,j-1}}{2}\right) - \beta_{j-1}\left(\frac{\psi_{i,j} + \psi_{i+1,j}}{2}\right)\right] \tag{4.21}$$

$$v^0_{i,j} = \frac{-1}{r_{j+\frac{1}{2}}\,\delta z_i}\left[\alpha_j\left(\frac{\psi_{i+1,j} - \psi_{i-1,j}}{2}\right) + \beta_j\left(\frac{\psi_{i+1,j+1} - \psi_{i-1,j+1}}{2}\right)\right]$$

On the other hand, the grid-point velocities may be derived by combining equations (4.16) and (4.17) as

Table 4.2 Weighting coefficients in equation (4.20)

j	α_j	β_j
1	3/4	1/4
2	7/12	5/12
3	11/20	9/20
4	15/28	13/28
5	19/36	17/36
6	23/44	21/44
7	27/52	25/52
>8	1/2	1/2

$$u_{i,j} = \frac{1}{2}\left(\frac{\psi_{i,j+1} - \psi_{i,j}}{r_{j+\frac{1}{2}}\Delta r_j} + \frac{\psi_{i,j} - \psi_{i,j-1}}{r_{j-\frac{1}{2}}\Delta r_{j-1}}\right)$$

(4.22)

$$v_{i,j} = \frac{1}{2}\left(-\frac{\psi_{i+1,j} - \psi_{i,j}}{r_j \Delta z_i} - \frac{\psi_{i,j} - \psi_{i-1,j}}{r_j \Delta z_{i-1}}\right)$$

The derivations given above permit the vorticity and velocity boundary conditions to be written as follows:

Vorticity Boundary Conditions.

$z = 0$

$$\omega_{i,j} = \frac{-2\psi_{2,j}}{r_j \Delta z_1^2} \tag{4.23}$$

$z = 1$

$$\omega_{1,j} = \frac{-2\psi_{1-\frac{1}{2},j}}{r_j \Delta z_{1-1}^2} \tag{4.24}$$

$r = 1$

$$\omega_{i,J} = \frac{-2A\psi_{i,J-1}}{r_{J-\frac{1}{2}} \Delta r_{J-1}^2} \tag{4.25}$$

Velocity Boundary Conditions

$r = 0$

$$u_{i,1} = \frac{\psi_{i,2}}{r_{1+\frac{1}{2}} \Delta r_1} \tag{4.26}$$

Note that the three vorticity equations given above are first-order accurate. However, they are the only ones that are consistent with the interior vorticity field and are able to satisfy the circulation theorem given earlier.

In the numerical computation that will be made later, equation (4.22) will be used to compute the grid-point velocities. Equation (4.21) will be used to compute the transport velocities for use in the convection terms in the vorticity transport equation (3.18) and the energy equation (3.22).

4.1.4 Generation of Nonuniform Grid System

For the convection problem under investigation, it is expected that there will be a boundary layer near the wall and a recirculating flow in the core region. It is desirable to use a nonuniform grid system such that a denser grid is formed in regions where both the flow and temperature fields change more rapidly. The method used to create a nonuniform grid in this work is the coordinate stretching technique.

Two stretching functions are used in this work. In the z direction, the stretching function used is [49]

$$\eta(z) = 0.5\left[1 + \tan\left[(2z-1)\,\frac{\pi\varepsilon}{2}\right]/\tan\frac{\pi\varepsilon}{2}\right] \qquad (4.27)$$

This function enables a mapping of z to η, ε being a deformation parameter--its presence controls the spacing of grid lines.

In practice, the velocity and temperature fields are solved numerically, it will be convenient if the indices used to represent

positions in the numerical computation can be related to the actual positions in the physical domain. The inverse of equation (4.27) is thus more useful and given as

$$z(\eta) = 0.5 + \frac{1}{\pi\varepsilon} \tan^{-1}\left[(2\eta-1) \tan \frac{\pi\varepsilon}{2}\right] \tag{4.28}$$

Examples of coordinate transformation constructed for $\varepsilon = 0.2$ and 0.9 are shown in Figure 4.3(a). The transformation of $\varepsilon = 0.2$ is close to being linear in that a uniform grid size in η is transformed to a uniform grid in z. For the present study, use of $\varepsilon = 0.2$ is adequate.

A different function is used to stretch grids in the r direction

$$\zeta(r) = a(e^{br} - 1) \tag{4.29}$$

This time a and b are deformation parameters, and for the present work, a and b are taken to be 0.044 and 3.1666, respectively. These values generate a grid system that has a coarse grid near $r = 0$. The grid lines become denser as they move close to the wall, see Figure 4.3(b).

The inverse of equation (4.30) is

$$r = \frac{1}{b} \ln \frac{\zeta + a}{a} \tag{4.30}$$

This equation enables the positions of r be found if ζ values are given.

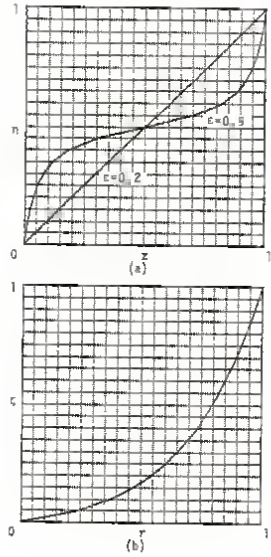

Figure 4.3 Stretching functions in (a) z direction and (b) r direction

A simultaneous use of equations (4.28) and (4.30) creates a 41X21 grid net as shown in Figure 4.4. This is the grid system used for numerical computation in the present study.

4.2 Solution Strategy

It is necessary to make decisions on (1) how to discretize the partial-differential governing equations given in Chapter III, and (2) how to solve these discretized equations numerically.

The first decision, in fact, has already been made in Section 4.1. As has been discussed there, a control-volume approach is able to yield a kinematically consistent velocity field. In addition, in formulating the boundary conditions for meeting continuous temperature and heat-flux conditions at the wall/insulation interface, an interface-diffusivity concept, equation (4.10), has also been employed. This concept is again developed based on the use of control-volume approach. This control-volume approach will be used consistently in formulating other finite-difference equations in this work [46,50].

As for the second decision on the selection of solution methods, two methods will be used for solving two kinds of equations. For example, the vorticity transport equation (3.18), the water energy equation (3.22), and the wall energy equation (3.26) all belong to the same type, namely, they are parabolic in time but elliptic in space. Such equations can be solved with several methods, the one that is chosen here is the Alternating Direction Implicit (ADI) method of Peaceman and Rachford [51]. In this method, each time step is split into two half steps, the space derivatives are approximated

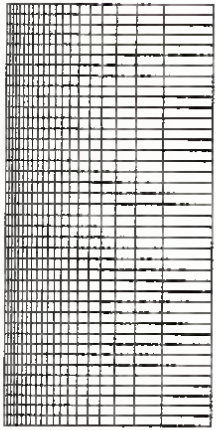

Figure 4.4 Grid system in water used in the present study

with both implicit- and explicit-difference schemes, alternating in each direction. Then the finite-difference equations can be expressed in a system of linear equations which can be organized in tridiagonal matrix forms suitable for solution with an efficient Thomas algorithm [50]. The ADI method is superior because it allows the use of large time steps to solve problems with a large number of equations [52].

It must be noted, however, that the water energy equation and the vorticity transport equation are both algebraically nonlinear in the unknowns, and this is because of the presence of convection terms which contain these unknowns in the coefficients expressed at new time. Linearization of these equations is necessary, and the method chosen is to evaluate these coefficients at old time--commonly known as lagging the coefficients [50]. In practice, the convection terms in the energy and vorticity transport equations are evaluated at old time, whereas the diffusion terms are split following the ADI method mentioned earlier. This hybrid scheme makes it possible to resolve the difficulty of nonlinearity while maintaining the transportive nature in those terms characterizing heat diffusion [36].

The stream function equation (3.19) is of elliptic type. For this equation, methods for solution are different and usually fall into two categories: direct and iterative. The direct method is limited to the solution of systems of small numbers of equations, the large round-off error inherent in this method also makes it unfavorable. The iterative method is therefore chosen. In addition,

a successive-over-relaxation (SOR) is employed in order to speed up convergence in the iteration.

CHAPTER V
FINITE DIFFERENCE EQUATIONS FOR GOVERNING EQUATIONS AND BOUNDARY CONDITIONS

The decisions made in Chapter IV on solution strategies will be used as guidance here in developing finite-difference approximations of the governing equations and boundary conditions given in Chapter III.

5.1 Finite-Difference Formulation for Energy Equation in Wall

The energy equation for wall has been given in Chapter III as follows:

$$\frac{\partial T_s}{\partial t} = \bar{a}\,\frac{\partial^2(\alpha T_s)}{\partial r_s^2} + \frac{\delta\bar{a}}{R_1 + \delta r_s}\,\frac{\partial(\alpha T_s)}{\partial r_s} + \frac{1}{A}\,\frac{\partial^2(\alpha T_s)}{\partial z^2} \tag{3.26}$$

The associated boundary conditions in the wall are

$$\begin{aligned} z = 0\ , &\qquad \frac{\partial T_s}{\partial z} = 0\ , \\ z = 1\ , &\qquad \frac{\partial T_s}{\partial z} = 0\ , \\ r_s = 0\ , &\qquad T_s(0,z,t) = T_1(z,t)\ , \end{aligned} \tag{3.27}$$

$$r_s = 1 \,, \qquad \frac{\partial T_s}{\partial r_s} + \frac{h_5}{k_s} T_s = 0$$

By integrating equation (3.26) over the control volume about point (i,j) (Figure 5.1) for a half-time step

$$\int_s^n \int_w^e \int_t^{t+\frac{\Delta t}{2}} \frac{\partial T_s}{\partial t} \Big)_{i,j} dt dr_s dz = \int_s^n \int_w^e \int_t^{t+\frac{\Delta t}{2}} B\Big[\frac{\partial}{\partial r_s}\Big(\frac{\partial (\alpha T_s)}{\partial r_s}\Big)\Big]_{i,j} dt dr_s dz$$

$$+ \int_s^n \int_w^e \int_t^{t+\frac{\Delta t}{2}} \Big[\frac{\partial (\alpha T_s)}{\partial r_s}\Big]_{i,j} \Big(\frac{\partial B}{R_1 + \delta r_s}\Big)_{i,j} dt dr_s dz$$

$$+ \int_s^n \int_w^e \int_t^{t+\frac{\Delta t}{2}} \frac{1}{\alpha}\Big[\frac{\partial}{\partial z}\Big(-\frac{\partial (\alpha T_s)}{\partial r_s}\Big)\Big]_{i,j} dt dr_s dz \qquad (5.1)$$

It is possible to derive the finite-difference approximation of the energy equation as

$$\frac{(T_s)^{k+\frac{1}{2}}_{i,j} - (T_s)^k_{i,j}}{\Delta t/2} = \frac{B}{\Delta r_s}\Big[(\alpha \frac{\partial T_s}{\partial r_s})^k_{i,j+\frac{1}{2}} - (\alpha \frac{\partial T_s}{\partial r_s})^k_{i,j-\frac{1}{2}}\Big]$$

$$+ \frac{\partial B}{\Delta r_s}\Big[\frac{\alpha}{R_1 + \delta r_{s,j}}\Big((T_s)^k_{i,j+\frac{1}{2}} - (T_s)^k_{i,j-\frac{1}{2}}\Big)\Big]$$

$$+ \frac{1}{\Delta r_z}\Big[(\alpha \frac{\partial T_s}{\partial z})^{k+\frac{1}{2}}_{i+\frac{1}{2},j} - (\alpha \frac{\partial T_s}{\partial z})^{k+\frac{1}{2}}_{i-\frac{1}{2},j}\Big]$$

(5.2)

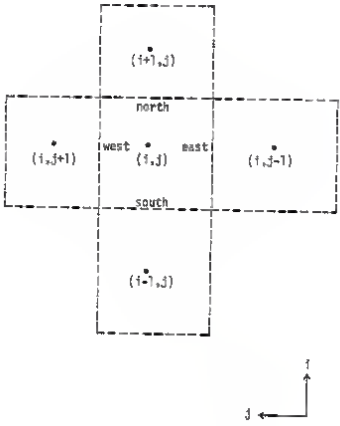

Figure 5.1 Notation for control-volume method

For this half-time step, the temperature is expressed explicitly in the r direction but implicitly in the z direction. According to the ADI method described in Chapter IV, for the next half-time step, the expression for these temperatures will be switched in that the temperature will be expressed explicitly in the z direction but implicitly in the r direction. Further development of finite-difference formulation in the wall will depend on how the wall is constructed.

5.1.1 Bare Wall

For a bare wall without insulation on it, the dimensionless diffusivity, α, that is the ratio of wall-diffusivity to water-diffusivity, is constant throughout the wall. Then, the temperature at the interface of two neighboring control volumes (Figure 5.1) may be approximated by an arithmetic mean

$$T_{i,j+\frac{1}{2}} = \frac{1}{2}(T_{i,j+1} + T_{i,j}) \tag{5.3}$$

and the temperature gradients approximated as

$$\left(\alpha \frac{\partial T}{\partial r}\right)_{i,j+\frac{1}{2}} = \alpha_{j+\frac{1}{2}} \frac{T_{i,j+1} - T_{i,j}}{\Delta r_s}$$

$$\left(\alpha \frac{\partial T}{\partial z}\right)_{i+\frac{1}{2},j} = \alpha_j \frac{T_{j+1,s} - T_{i,j}}{\Delta z_i} \tag{5.4}$$

With the substitution of these relations and dropping subscript s of 1 for simplicity sake, equation (5.2) is changed to

$$\left(\frac{-\alpha}{\Delta\forall z_i \Delta z_{i-1}}\right)T^{k+\frac{1}{2}}_{i-1,j} + \left(\frac{2}{\Delta t} + \frac{\alpha}{\Delta\forall z_i \Delta z_i} + \frac{\alpha}{\Delta\forall z_i \Delta z_{i-1}}\right)T^{k+\frac{1}{2}}_{i,j} + \left(\frac{-\alpha}{\Delta\forall z_i \Delta z_i}\right)T^{k+\frac{1}{2}}_{i+1,j}$$

$$= \left(\frac{\alpha\theta}{\Delta r^2} - \frac{\alpha\theta}{2\Delta r(R_i + \Delta r_j)}\right)T^{k}_{i,j-1} + \left(\frac{2}{\Delta t} - \frac{2\alpha\theta}{\Delta r^2}\right)T^{k}_{i,j}$$

$$+ \left(\frac{\alpha\theta}{\Delta r^2} + \frac{\alpha\theta}{2\Delta r(R_i + \Delta r_j)}\right)T^{k}_{i,j+1} \qquad (5.5)$$

This equation can be expressed compactly as

$$(-\alpha C_{11})T^{k+\frac{1}{2}}_{i-1,j} + \left(\frac{2}{\Delta t} + \alpha C_{11} + \alpha C_{12}\right)T^{k+\frac{1}{2}}_{i,j} + (\alpha C_{12})T^{k+\frac{1}{2}}_{i+1,j}$$

$$= (C_{13} - C_{14})T^{k}_{i,j-1} + \left(\frac{2}{\Delta t} - 2C_{13}\right)T^{k}_{i,j} + (C_{13} + C_{14})T^{k}_{i,j+1} \qquad (5.6)$$

where coefficients C_{11} through C_{14} are defined in Table 5.1.

In the derivation given above, equation (5.6) was obtained by integrating equation (3-26); this same equation (5.6) may be derived by using Taylor's series, as is not unexpected.

For the second half-time step, the finite-difference equation for T can be derived as

$$(-C_{13} + C_{14})T^{k+1}_{i,j-1} + \left(\frac{2}{\Delta t} + 2C_{13}\right)T^{k+1}_{i,j} + (-C_{13} - C_{14})T^{k}_{i,j+1}$$

$$= (\alpha C_{11})T^{k+\frac{1}{2}}_{i-1,j} + \left(\frac{2}{\Delta t} - \alpha C_{11} - \alpha C_{12}\right)T^{k+\frac{1}{2}}_{i,j} + (\alpha C_{12})T^{k+\frac{1}{2}}_{i+1,j} \qquad (5.7)$$

Table 5.1 Definitions for C coefficients

$$C_9 = \frac{1}{r_{j+\frac{1}{2}} \Delta r_j \forall r_j}$$

$$C_{10} = \frac{1}{r_{j-\frac{1}{2}} \forall r_j \Delta r_j}$$

$$C_{11} = \frac{1}{A \forall z_i \Delta z_{i-1}}$$

$$C_{12} = \frac{1}{A \forall z_i \Delta z_i}$$

$$C_{13} = \frac{\alpha \delta}{\Delta r_s^2}$$

$$C_{14} = \frac{\alpha \delta^2}{2 \Delta r_s (R_i + \Delta r_s)}$$

$$C_{15} = 2C_{13} - (C_{13} + C_{14}) \frac{1}{1 + \frac{h \delta \Delta r_s}{k_s}}$$

$$C_{16} = \frac{a_1}{2 \forall z_i}$$

$$C_{17} = \frac{a_2}{2 \forall z_i}$$

$$C_{18} = \frac{a_3}{2 \forall z_i}$$

$$C_{19} = \frac{A r_{j-\frac{1}{2}}}{r_j \forall r_j \Delta r_{j-1}} + \frac{a_4 r_{j-\frac{1}{2}}}{2 r_j \forall r_j}$$

Table 5.1-continued

$$C_{20} = \frac{Ar_{j+\frac{1}{2}}}{r_j \forall r_j \Delta r_j} + \frac{Ar_{j-\frac{1}{2}}}{r_j \forall r_j \Delta r_{j-1}} + \frac{a_5 r_{j+\frac{1}{2}} + a_6 r_{j-\frac{1}{2}}}{2r_j \forall r_j}$$

$$C_{21} = \frac{Ar_{j+\frac{1}{2}}}{r_j \forall r_j \Delta r_j} - \frac{a_4 r_{j+\frac{1}{2}}}{2r_j \forall r_j}$$

$$C_{22} = \frac{2A}{\Delta r^2_{j-1}} + \frac{a_7 r_{j-\frac{1}{2}}}{2r_j \Delta r_{j-1}}$$

$$C_{23} = \frac{2A}{\Delta r^2_{j-1}} + \frac{a_6 r_{j-\frac{1}{2}}}{2r_j \Delta r_{j-1}}$$

$$C_{24} = -PrC_{11} - C_{18}$$

$$C_{25} = PrC_{11} + PrC_{12} + C_{17}$$

$$C_{26} = -PrC_{12} + C_{16}$$

$$C_{27} = \frac{a_7}{2\forall r_j} + \frac{APr\, r_{j-1}}{r_{j-\frac{1}{2}} \forall r_j \Delta r_{j-1}}$$

$$C_{28} = \frac{-a_5 + a_6}{2\forall r_j} + \frac{APr\, r_j}{r_{j+\frac{1}{2}} \forall r_j \Delta r_j} - \frac{APr\, r_j}{r_{j-\frac{1}{2}} \forall r_j \Delta r_{j-1}}$$

$$C_{29} = \frac{-a_4}{2\forall r_j} + \frac{APr\, r_{j+1}}{r_{j+\frac{1}{2}} \forall r_j \Delta r_j}$$

$$C_{30} = \frac{RaPr}{2A\forall r_j}$$

Table 5.1-continued.

where $a_1 = u_n = |u_n|$

$a_2 = u_n + |u_n| - u_s + |u_s|$

$a_3 = u_s + |u_s|$

$a_4 = v_w - |v_w|$

$a_5 = v_w + |v_w|$

$a_6 = -v_e + |v_e|$

$a_7 = v_e + |v_e|$

u_n, u_s, v_e and v_w are defined in equation (4.21)

$\forall z_i$, Δz_i, $\forall r_j$, Δr_j are defined below and shown in Figure 4.2

other variables are defined in NOMENCLATURE

$\forall z_i = (z_{i+1} - z_{i-1})/2$

$\Delta z_i = z_{i+1} - z_i$

$\forall r_j = (r_{j+1} - r_{j-1})/2$

$\Delta r_j = r_{j+1} - r_j$

5.1.2 Insulated Wall

For a tank wall with insulation on it, temperatures for interior grid points in wall (or insulation) will be treated just like these grid points in a bare wall but will use correct properties to account for material variation. For those points adjacent to the wall/insulation interface, however, special care must be taken to account for material property variation across the interface.

Consider the grid point located to the right of the interface shown in Figure 5.2(a). It is obvious from equation (5.2) that

$$\left(\alpha \frac{\partial T}{\partial r}\right)_{i,j+\frac{1}{2}} = \alpha_{j+\frac{1}{2}} \frac{T_{i,j+1} - T_{i,j}}{\Delta r}$$

$$\left(\alpha \frac{\partial T}{\partial r}\right)_{i,j-\frac{1}{2}} = \alpha_{j-\frac{1}{2}} \frac{T_{i,j} - T_{i,j-1}}{\Delta r} \qquad (5.8)$$

$$\left(\alpha \frac{\partial T}{\partial z}\right)_{i+\frac{1}{2},j} = \alpha_{j} \frac{T_{i+1,j} - T_{i,j}}{\Delta z_i}$$

Here α_j and $\alpha_{j-\frac{1}{2}}$ stand for dimensionless diffusivity of material 1 because the dashed-line boundaries separating the control volumes to the right of the interface are all located in material 1. The diffusivity $\alpha_{j+\frac{1}{2}}$, however, is different, this diffusivity is defined as the ratio of the 'interface' diffusivity (equation (4.10)) to water diffusivity.

The same distinction must be made in temperature expressions. While $T_{i,j-\frac{1}{2}}$ can be approximated as the arithmetic mean of

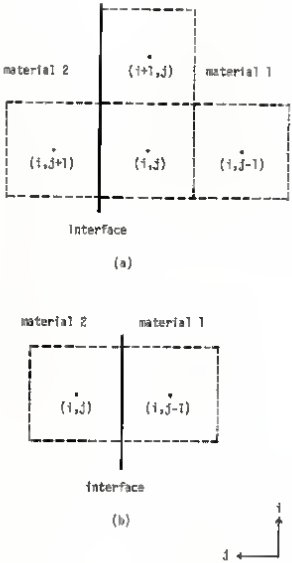

Figure 5.2 Treatment of grid points adjacent to interface

neighboring temperatures $T_{i,j}$ and $T_{i,j-1}$. $T_{i,j+\frac{1}{2}}$ must be expressed differently. In order to satisfy continous heat fluxes at wall/water interface, the 'interface' temperature $T_{i,j+\frac{1}{2}}$ must meet similar requirement of flux continuity, thus satisfying

$$T_{i,j+\frac{1}{2}} = \frac{T_{i,j} + \frac{k_2}{k_1} T_{i,j+1}}{1 + \frac{k_2}{k_1}} \tag{5.9}$$

With the substitution of these new relations, equation (5.2) takes the following form:

$$(-\alpha C_{11})T^{k+\frac{1}{2}}_{i-1,j} + (\frac{2}{\Delta t} + \alpha C_{11} + \alpha C_{12})T^{k+\frac{1}{2}}_{i,j} + (\alpha C_{12})T^{k+\frac{1}{2}}_{i+1,j}$$

$$= (C_{13} - C_{14})T^{k}_{i,j-1} + (\frac{2}{\Delta t} - C_{13} - C^*_{13} - C_{14} + C^*_{14})T^{k}_{i,j}$$

$$+ (C^*_{13} + C^*_{15})T^{k}_{i,j+1} \tag{5.10}$$

where C_{11} through C_{14} are again defined as in Table 5.1. Those C^*_{13} through C^*_{15} are defined as follows

$$C^*_{13} = \frac{\alpha^*\theta}{\Delta r^2}$$

$$C^*_{14} = \frac{2C_{14}}{1+(k_2/k_1)}$$

$$C^*_{15} = \frac{2C_{14}(k_2/k_1)}{1+(k_2/k_1)} \tag{5.11}$$

In these relations, α^* is the interface diffusivity ratio, as has been defined previously.

For the second half-time step, the finite-difference equation for T can be derived as

$$(-C_{13}+C_{14})T^{k+1}_{i,j-1} + (\frac{2}{\Delta t}+C_{13}+C^*_{13}+C_{14}-C^*_{14})T^{k+1}_{i,j} + (-C^*_{13}-C^*_{15})T^{k+1}_{i,j+1}$$

$$= (\alpha C_{11})T^{k+\frac{1}{2}}_{i-1,j} + (\frac{2}{\Delta t}+\alpha C_{11}+\alpha C_{12})T^{k+\frac{1}{2}}_{i,j} + (\alpha C_{12})T^{k+\frac{1}{2}}_{i+1,j} \qquad (5.12)$$

The derivation given above for an insulated wall is for a grid point located to the right of the interface (Figure 5.2(a)). For the grid point located to the left of the interface, Figure 5.2(b), a slight modification of the formulation is in order. This time $\alpha_{j-1/2}$ strides across two different materials and thus becomes the interface diffusivity. Correspondingly, $T_{i,j-1/2}$ is the interface temperature as defined previously. For this grid point, the first half-time step and second half-time step finite-difference equations are respectively

$$(-\alpha C_{11})T^{k+\frac{1}{2}}_{i-1,j} + (\frac{2}{\Delta t}+\alpha C_{11}+\alpha C_{12})T^{k+\frac{1}{2}}_{i,j} + (\alpha C_{12})T^{k+\frac{1}{2}}_{i+1,j}$$

$$= (C^*_{13}-C^*_{14})T^{k}_{i,j-1} + (\frac{2}{\Delta t}-C^*_{13}-C_{13}+C_{14}-C^*_{15})T^{k}_{i,j} + (C_{13}+C_{14})T^{k}_{i,j+1}$$

(5.13)

$$(-C^*_{13}+C^*_{14})T^{k+1}_{i,j-1} + (\frac{2}{\Delta t}+C_{13}+C^*_{13}-C_{14}+C^*_{15})T^{k+1}_{i,j} + (-C_{13}-C_{14})T^{k+1}_{i,j+1}$$

$$= (\alpha C_{11})T_{i-1,j}^{k+\frac{1}{2}} + (\frac{2}{\Delta t} - \alpha C_{11} - \alpha C_{12})T_{i,j}^{k+\frac{1}{2}} + (-\alpha C_{12})T_{i+1,j}^{k+\frac{1}{2}} \qquad (5.14)$$

where the definitions for coefficients remain unchanged.

The finite-difference formulation for governing equations in the wall is now complete. Attention is now directed to the boundary conditions in the wall.

For grid points located at the air/wall interface, Figure 5.3, the boundary condition for T is

$$T_{i,j} = \frac{T_{i,j-1}}{1 + \frac{h_i \Delta r}{k_s}} \qquad (5.15)$$

For grid points along the top and bottom boundaries of the wall, the adiabatic condition there requires that the following condition be met

$$\begin{aligned} T_{1,j} &= T_{2,j} \\ T_{l,j} &= T_{l-1,j} \end{aligned} \qquad (5.16)$$

Along the wall/water interface, the boundary temperature must satisfy

$$T_{i,1} = T_{interface} \qquad (5.17)$$

These boundary conditions may be incorporated into the finite-difference energy equations derived earlier for the wall and to

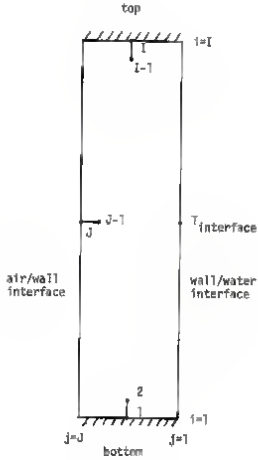

Figure 5.3 Wall region temperature boundary conditions

simplify those equations that contain grid-point temperatures adjacent to the boundaries. These difference energy equations are then solved and once the temperatures at interior points are found numerically, the boundary temperatures may be recomputed using the boundary conditions given above.

5.1.3 Summary in Matrix Forms

The finite-difference governing equations derived above may be expressed in matrix forms, as will now be shown. In general, the temperatures in the wall are found by solving the matrix equation

$$\bar{\bar{A}}\,\bar{C} = \bar{B} \tag{5.18}$$

Matrix A and vectors B and C in this equation vary with time steps and also the way the wall is constructed.

(1) For a bare wall without insulation on it, at the first half-time step,

$$\bar{\bar{A}} = \begin{vmatrix} (\frac{2}{\Delta t}+\alpha C_{12}) & (-\alpha C_{12}) & & & & \\ (-\alpha C_{11}) & (\frac{2}{\Delta t}+\alpha C_{11}+\alpha C_{12}) & (-\alpha C_{12}) & & & \\ & \ddots & \ddots & \ddots & & \\ & & & (-\alpha C_{11}) & (\frac{2}{\Delta t}+\alpha C_{11}+\alpha C_{12}) & (-\alpha C_{12}) \\ & & & & (-\alpha C_{11}) & (\frac{2}{\Delta t}+\alpha C_{11}) \end{vmatrix} \tag{5.19a}$$

$\bar{B}$: $j = 2,3,\ldots,J-2$

$$\begin{vmatrix} (C_{13}-C_{14})T^k_{2,j-1} + (\frac{2}{\Delta t} - 2C_{13})T^k_{2,j} + (C_{13}+C_{14})T^k_{2,j+1} \\ \vdots \\ (C_{13}-C_{14})T^k_{I-1,j-1} + (\frac{2}{\Delta t} - 2C_{13})T^k_{I-1,j} + (C_{13}+C_{14})T^k_{I-1,j+1} \end{vmatrix} \tag{5.19b}$$

$j = J-1$

$$\begin{vmatrix} (C_{13}-C_{14})T^k_{2,j-1} + (\frac{2}{\Delta t} - C_{15})T^k_{2,j} \\ \vdots \\ (C_{13}-C_{14})T^k_{I-1,j-1} + (\frac{2}{\Delta t} - C_{15})T^k_{I-1,j} \end{vmatrix}$$

$\bar{C}$: $j = 2,3,\ldots,J-1$

$$\begin{vmatrix} T^{k+\frac{1}{2}}_{2,j} \\ \vdots \\ T^{k+\frac{1}{2}}_{I-1,j} \end{vmatrix} \tag{5.19c}$$

At the second half-time step,

$$\bar{A} = \begin{vmatrix} (\frac{2}{\Delta t}+2C_{13}) & (-C_{13}-C_{14}) & & & \\ (-C_{13}+C_{14}) & (\frac{2}{\Delta t}+2C_{13}) & (-C_{13}-C_{14}) & & \\ & \ddots & \ddots & \ddots & \\ & & (-C_{13}+C_{14}) & (\frac{2}{\Delta t}+2C_{13}) & (-C_{13}-C_{14}) \\ & & & (-C_{13}+C_{14}) & (\frac{2}{\Delta t}+2C_{15}) \end{vmatrix} \tag{6.20a}$$

$\bar{B}$ $i = 2$

$$\begin{vmatrix} (\frac{2}{\Delta t}-\alpha C_{12})T_{i,2}^{k+\frac{1}{2}} + (\alpha C_{12})T_{i+1,2}^{k+\frac{1}{2}} - (-C_{13}+C_{14})T_{i,1}^{k+1} \\ (\frac{2}{\Delta t}-\alpha C_{12})T_{i,3}^{k+\frac{1}{2}} + (\alpha C_{12})T_{i+1,3}^{k+\frac{1}{2}} \\ \vdots \\ (\frac{2}{\Delta t}-\alpha C_{12})T_{i,J-1}^{k+\frac{1}{2}} + (\alpha C_{12})T_{i+1,J-1}^{k+\frac{1}{2}} \end{vmatrix}$$

$i = 3,4,\ldots,I-2$

$$\begin{vmatrix} (\alpha C_{11})T_{i-1,2}^{k+\frac{1}{2}} + (\frac{2}{\Delta t}-\alpha C_{11}-\alpha C_{12})T_{i,2}^{k+\frac{1}{2}} + (\alpha C_{12})T_{i+1,2}^{k+\frac{1}{2}} - (-C_{13}+C_{14})T_{i,1}^{k+1} \\ (\alpha C_{11})T_{i-1,3}^{k+\frac{1}{2}} + (\frac{2}{\Delta t}-\alpha C_{11}-\alpha C_{12})T_{i,3}^{k+\frac{1}{2}} + (\alpha C_{12})T_{i+1,3}^{k+\frac{1}{2}} \\ \vdots \\ (\alpha C_{11})T_{i-1,J-1}^{k+\frac{1}{2}} + (\frac{2}{\Delta t}-\alpha C_{11}-\alpha C_{12})T_{i,J-1}^{k+\frac{1}{2}} + (\alpha C_{12})T_{i+1,J-1}^{k+\frac{1}{2}} \end{vmatrix}$$

(5.20b)

$i = I-1$

$$\begin{vmatrix} (\alpha C_{11})T_{I-1,2}^{k+\frac{1}{2}} + (\frac{2}{\Delta t} - \alpha C_{11})T_{I,2}^{k+\frac{1}{2}} - (-C_{13}+C_{14})T_{I,1}^{k+1} \\ (\alpha C_{11})T_{I-1,3}^{k+\frac{1}{2}} + (\frac{2}{\Delta t} - \alpha C_{11})T_{I,3}^{k+\frac{1}{2}} \\ \vdots \\ (\alpha C_{11})T_{I-1,J-1}^{k+\frac{1}{2}} + (\frac{2}{\Delta t} - \alpha C_{11})T_{I,J-1}^{k+\frac{1}{2}} \end{vmatrix}$$

$\vec{C}$; $i = 2,3,\ldots,I-1$

$$\begin{vmatrix} T_{I,2}^{k+1} \\ \vdots \\ T_{I,J-1}^{k+1} \end{vmatrix} \qquad (5.20c)$$

where C_{11} through C_{14} have been defined in Table 5.1. It is clear that both A matrices given in equations (5.19a) and (5.20a) are tridiagonal, a form enabling the matrix equation (5.18) to be solved by efficient Thomas algorithm, as mentioned in Chapter IV.

(2) For an insulated wall, at first half-time step, matrix A is unchanged from that of the bare wall at the same time-step. Likewise, vector B follows much the same form as before, except for those two grid lines adjacent to the wall/insulation interface. Say the interface is located between $j = j-1$ and $j = j+1$, then

$\bar{B}$: j = j-1

$$\begin{vmatrix} (C_{13}-C_{14})T^k_{2,j-1} + (\frac{2}{\Delta t} - C_{13} - C^*_{13} - C_{14} + C^*_{14})T^k_{2,j} + (C^*_{13}+C^*_{15})T^k_{2,j+1} \\ \vdots \\ (C_{13}-C_{14})T^k_{I-1,j-1} + (\frac{2}{\Delta t} - C_{13} - C^*_{13} - C_{14} + C^*_{14})T^k_{I-1,j} + (C^*_{13}+C^*_{15})T^k_{I-1,j+1} \end{vmatrix} \tag{5.21a}$$

j = j+1

$$\begin{vmatrix} (C^*_{13}-C^*_{14})T^k_{i,j-1} + (\frac{2}{\Delta t} - C_{13} - C^*_{13} + C_{14} - C^*_{15})T^k_{i,j} + (C_{13}+C_{14})T^k_{i,j+1} \\ \vdots \\ (C^*_{13}-C^*_{14})T^k_{I-1,j-1} + (\frac{2}{\Delta t} - C_{13} - C^*_{13} + C_{14} - C^*_{15})T^k_{I-1,j} + (C_{13}+C_{14})T^k_{I-1,j+1} \end{vmatrix} \tag{5.21b}$$

At second half-time step, vector $\bar{B}$ is unchanged from that of the bare wall at the same time-step. Matrix A is changed as follows

$$
\left|
\begin{array}{l}
(\frac{2}{\Delta t}+2C_{13}) \quad (-C_{13}-C_{14}) \\
(-C_{13}+C_{14}) \quad (\frac{2}{\Delta t}+2C_{13}) \quad (-C_{13}-C_{14}) \\
\quad \ddots \qquad \ddots \qquad \ddots \\
\quad (-C_{13}+C_{14}) \quad (\frac{2}{\Delta t}+2C_{13}) \quad (-C_{13}-C_{14}) \\
\quad (-C_{13}+C_{14}) \quad (\frac{2}{\Delta t}+C_{13}+C_{13}^{*}+C_{14}-C_{14}^{*}) \quad (-C_{13}^{*}-C_{15}^{*}) \\
\hdashline
\qquad (-C_{13}^{*}+C_{14}^{*}) \quad (\frac{2}{\Delta t}+C_{13}+C_{13}^{*}+C_{15}^{*}-C_{14}) \quad (-C_{13}-C_{14}) \\
\qquad\qquad (-C_{13}+C_{14}) \quad (\frac{2}{\Delta t}+2C_{13}) \quad (-C_{13}-C_{14}) \\
\qquad\qquad\quad \ddots \qquad \ddots \qquad \ddots \\
\qquad\qquad\qquad (-C_{13}+C_{14}) \quad (\frac{2}{\Delta t}+2C_{13}) \quad (-C_{13}-C_{14}) \\
\qquad\qquad\qquad\qquad (-C_{13}+C_{14}) \quad (\frac{2}{\Delta t}+C_{15})
\end{array}
\right|
$$

Interface (dashed line)

(5.22)

5.2 Finite-Difference Formulation for Energy Equation in Water

The energy equation in water has been given in Chapter III as

$$\frac{\partial T_f}{\partial t} + \frac{1}{r_f}\frac{\partial}{\partial r_f}(r_f v T_t) + \frac{\partial}{\partial z}(uT_f) = A[\frac{1}{r_f}\frac{\partial}{\partial r_f}(r_f \frac{\partial T_f}{\partial r_f})] + \frac{1}{A}\frac{\partial^2 T_f}{\partial z^2} \qquad (3.22)$$

The associated boundary conditions in water are

$$
\begin{aligned}
z = 0 , \qquad & \frac{\partial T_f}{\partial z} = 0 , \\
z = 1 , \qquad & \frac{\partial T_f}{\partial z} = 0 , \\
r_f = 0 , \qquad & \frac{\partial T_f}{\partial r_f} = 0 , \\
r_f = 1 , \qquad & T_f(1,z,t) = T_j(z,t)
\end{aligned}
\tag{3,23}
$$

The finite-difference energy equation in water may be derived following the same procedure used before for the wall and the result is

$$
\frac{T^{k+\frac{1}{2}}_{i,j} - T^{k}_{i,j}}{\Delta t/2} + \frac{1}{r_j \Delta r_j}\left[(rvT)^{k}_{i,j+\frac{1}{2}} - (rvT)^{k}_{i,j-\frac{1}{2}}\right]
$$

$$
+ \frac{1}{\Delta z_i}\left[(n^{k}T^{k+\frac{1}{2}})_{i+\frac{1}{2},j} - (n^{k}T^{k+\frac{1}{2}})_{i-\frac{1}{2},j}\right]
$$

$$
= \frac{A}{r_j \Delta r_j}\left[(r\frac{\partial T}{\partial r})^{k}_{i,j+\frac{1}{2}} - (r\frac{\partial T}{\partial r})^{k}_{i,j-\frac{1}{2}}\right] + \frac{1}{A\Delta z_i}\left[(\frac{\partial T}{\partial z})^{k+\frac{1}{2}}_{i+\frac{1}{2},j} - (\frac{\partial T}{\partial z})^{k+\frac{1}{2}}_{i-\frac{1}{2},j}\right]
\tag{5,23}
$$

This equation is derived for temperatures of water at the first half-time step, here the temperature is expressed explicitly in the r direction but implicitly in the z direction. Velocity coefficients,

being taken at old times, are 'lagged' in the computation, as described in Chapter IV.

A second-upwind differencing scheme is used to treat the convection terms in equation (5.23). Referring to Figure 5.4,

$$(uT)_{i+\frac{1}{2},j} - (uT)_{i-\frac{1}{2},j} = \tfrac{1}{2}\{[(u_n-|u_n|)T_{i+1,j} + (u_n+|u_n|)T_{i,j}] - [(u_s-|u_s|)T_{i,j} + (u_s+|u_s|)T_{i-1,j}]\} \tag{5.24}$$

$$(rvT)_{i,j+\frac{1}{2}} - (rvT)_{i,j-\frac{1}{2}} = \tfrac{1}{2}\{r_{j+\frac{1}{2}}[(v_e-|v_e|)T_{i,j+1} + (v_e+|v_e|)T_{i,j}] - r_{j-\frac{1}{2}}[(v_w-|v_w|)T_{i,j} + (v_w+|v_w|)T_{i,j-1}]\}$$

Here u_s, u_n, v_e and v_w refer to old-time transport velocities defined by equation (4.21). With the use of these two relations, equation (5.23) is changed to

$$(-C_{11}-C_{18})T^{k+\frac{1}{2}}_{i-1,j} + (\tfrac{2}{\Delta t}+C_{11}+C_{12}+C_{17})T^{k+\frac{1}{2}}_{i,j} + (C_{16}-C_{12})T^{k+\frac{1}{2}}_{i+1,j} = C_{19}T^{k}_{i,j-1} + (\tfrac{2}{\Delta t}-C_{20})T^{k}_{i,j} + C_{21}T^{k}_{i,j+1} \tag{5.25}$$

where C_{11}, C_{12} and C_{16} through C_{21} have been defined in Table 5.1.

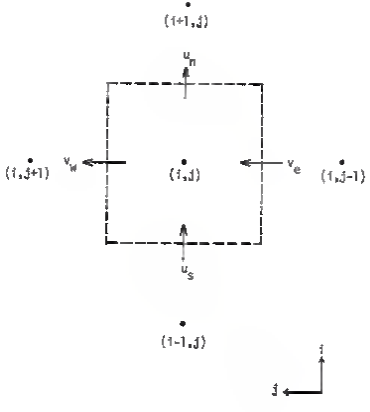

Figure 5.4 Second upwind difference scheme

For the second half-time step,

$$(-C_{19})T_{i,j-1}^{k+1} + (\frac{2}{\Delta t} + C_{20})T_{i,j}^{k+1} + (-C_{21})T_{i,j+1}^{k+1}$$

$$= (C_{11}+C_{18})T_{i-1,j}^{k+\frac{1}{2}} + (\frac{2}{\Delta t} - C_{11} - C_{12} - C_{17})T_{i,j}^{k+\frac{1}{2}} + (C_{12} - C_{16})T_{i+1,j}^{k+\frac{1}{2}} \tag{5.26}$$

The formulation of the finite-difference energy equation for water is now complete. Attention is now directed to the boundary conditions in water as follows:

For grid points at the centerline of the tank, Figure 5.5,

$$T_{i,1} = T_{i,2} \tag{5.27}$$

For grid points located at the top and bottom boundaries,

$$T_{1,j} = T_{2,j}$$

$$T_{I,j} = T_{I-1,j} \tag{5.28}$$

For grid points at the wall/water interface,

$$T_{i,J} = T_{\text{interface}} \tag{5.29}$$

Once again, these conditions are incorporated into the finite-difference energy equations for water, and these equations are solved for interior temperatures. Once these interior temperatures are

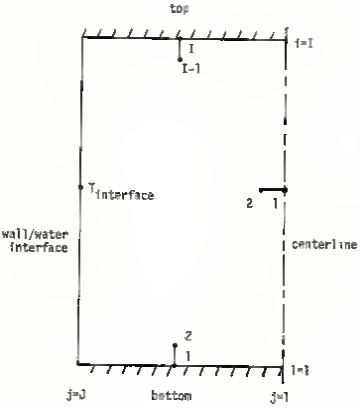

Figure 5.5 Water region temperature boundary conditions

found, the boundary temperatures of water can be obtained by using these boundary conditions given above.

It is again desirable to summarize the governing equations derived above for water in matrix expressions. In general, the interior temperatures of water are found by solving

$$\bar{\bar{A}}\,\bar{C} = \bar{B} \tag{5.30}$$

The matrix A and vectors B and C are defined differently for different time steps. For example, at the first half-time step,

$$\bar{\bar{A}} = \begin{vmatrix} (\frac{2}{\Delta t}+C_{12}+C_{17}-C_{18}) & (C_{16}-C_{12}) & & & \\ (-C_{18}-C_{11}) & (\frac{2}{\Delta t}+C_{11}+C_{12}+C_{17}) & (C_{16}-C_{12}) & & \\ & \ddots & \ddots & \ddots & \\ & & (-C_{18}-C_{11}) & (\frac{2}{\Delta t}+C_{11}+C_{12}+C_{17}) & (C_{16}-C_{12}) \\ & & & (-C_{18}-C_{11}) & (\frac{2}{\Delta t}+C_{11}+C_{12}+C_{17}) \end{vmatrix} \tag{5.31a}$$

$$\bar{B} \quad j = 2$$

$$\begin{vmatrix} (\frac{2}{\Delta t}+C_{19}-C_{20})T^k_{2,j} + C_{21}T^k_{2,j+1} \\ \vdots \\ (\frac{2}{\Delta t}+C_{19}-C_{20})T^k_{I-1,j} + C_{21}T^k_{I-1,j+1} \end{vmatrix} \tag{5.31b}$$

$j = 3,4,\ldots,J-1$

$$\begin{vmatrix} C_{19}T^k_{2,j-1} + (\frac{2}{\Delta t} - C_{20})T^k_{2,j} + C_{21}T^k_{2,j+1} \\ \vdots \\ C_{19}T^k_{I-1,j-1} + (\frac{2}{\Delta t} - C_{20})T^k_{I-1,j} + C_{21}T^k_{I-1,j+1} \end{vmatrix}$$

$\bar{C}$: $j = 2,3,\ldots,J-1$

$$\begin{vmatrix} T^{k+\frac{1}{2}}_{2,j} \\ \vdots \\ T^{k+\frac{1}{2}}_{I-1,j} \end{vmatrix} \qquad (5.31c)$$

At the second half-time step, they become

$\bar{\bar{A}}$.

$$\begin{vmatrix} (\frac{2}{\Delta t} + C_{20} - C_{19}) & (-C_{21}) & & & \\ (-C_{19}) & (\frac{2}{\Delta t} + C_{20}) & (-C_{21}) & & \\ & \ddots & \ddots & \ddots & \\ & & (-C_{19}) & (\frac{2}{\Delta t} + C_{20}) & (-C_{21}) \\ & & & (-C_{19}) & (\frac{2}{\Delta t} + C_{20}) \end{vmatrix} \qquad (5.32a)$$

$\bar{\theta}$: $i = 2$

$$\begin{vmatrix} (\frac{2}{\Delta t} - C_{12} - C_{17} + C_{18})T_{i,2}^{k+\frac{1}{2}} + (C_{12} - C_{16})T_{i+1,2}^{k+\frac{1}{2}} \\ \vdots \\ (\frac{2}{\Delta t} - C_{12} - C_{17} + C_{18})T_{i,J-2}^{k+\frac{1}{2}} + (C_{12} - C_{16})T_{i+1,J-2}^{k+\frac{1}{2}} \\ (\frac{2}{\Delta t} - C_{12} - C_{17} + C_{18})T_{i,J-1}^{k+\frac{1}{2}} + (C_{12} - C_{16})T_{i+1,J-1}^{k+\frac{1}{2}} + C_{21}T_{i,J}^{k+1} \end{vmatrix}$$

$i = 3, 4, \ldots, I-2$

$$\begin{vmatrix} (C_{11} + C_{18})T_{i-1,2}^{k+\frac{1}{2}} + (\frac{2}{\Delta t} - C_{11} - C_{12} - C_{17})T_{i,2}^{k+\frac{1}{2}} + (C_{12} - C_{16})T_{i+1,2}^{k+\frac{1}{2}} \\ \vdots \\ (C_{11} + C_{18})T_{i-1,J-2}^{k+\frac{1}{2}} + (\frac{2}{\Delta t} - C_{11} - C_{12} - C_{17})T_{i,J-2}^{k+\frac{1}{2}} + (C_{12} - C_{16})T_{i+1,J-2}^{k+\frac{1}{2}} \\ (C_{11} + C_{18})T_{i-1,J-1}^{k+\frac{1}{2}} + (\frac{2}{\Delta t} - C_{11} - C_{12} - C_{17})T_{i,J-1}^{k+\frac{1}{2}} + (C_{12} - C_{16})T_{i+1,J-1}^{k+\frac{1}{2}} + C_{21}T_{i,J}^{k+1} \end{vmatrix}$$

(5.32b)

$i = 1+1$

$$\begin{vmatrix} (C_{11}+C_{18})T_{i-1,2}^{k+\frac{1}{2}} + (\frac{2}{\Delta t}-C_{11}-C_{16}-C_{17})T_{i,2}^{k+\frac{1}{2}} \\ \vdots \\ (C_{11}+C_{18})T_{i-1,J-2}^{k+\frac{1}{2}} + (\frac{2}{\Delta t}-C_{11}-C_{16}-C_{17})T_{i,J-2}^{k+\frac{1}{2}} \\ (C_{11}+C_{18})T_{i-1,J-1}^{k+\frac{1}{2}} + (\frac{2}{\Delta t}-C_{11}-C_{16}-C_{17})T_{i,J-1}^{k+\frac{1}{2}} + C_{21}T_{i,J}^{k+1} \end{vmatrix}$$

$\bar{C}$: $i = 2,3,\ldots,I-1$

$$\begin{vmatrix} T_{i,2}^{k+1} \\ \vdots \\ T_{i,J-1}^{k+1} \end{vmatrix} \qquad (5.32c)$$

Coefficients C_{11}, C_{12} and C_{16} through C_{21} have been defined in Table 5.1. Again note that the two A matrices given are tridiagonal.

5.3 Iterative Solution for Two Energy Equations

Both energy equations for wall and water must be solved simultaneously to satisfy continuity of temperatures and heat fluxes at the wall/water interface. It is anticipated that many iterations are needed to obtain convergent temperatures at each time step. In this effort, the already convergent, previous time-step temperatures (for example, temperature vectors in equations (5.19b) and (5.31b)), are assigned fixed at each iteration and new temperatures at k+(1/2)

and k+1 at the same grid locations are computed, iterated, and tested until they converge. Each time during iteration, the interface temperature is modified by using equation (4.3) and the temperature convergence is hinged on a convergent heat flux

$$\underset{i}{\text{Max}} \left| \frac{q_{f,i} - q_{s,i}}{\frac{q_{f,i} + q_{s,i}}{2}} \right| \leq 10^{-3} \tag{5.33}$$

where the interface grid locations are indexed as i, i=1 through I. Heat fluxes q_f and q_s refer to those in the water and the wall, respectively.

5.4 Finite-Difference Formulation for Vorticity Transport Equation

The vorticity transport equation has been given in Chapter III as

$$\frac{\partial \omega}{\partial t} + \frac{\partial}{\partial r_f}(v\omega) + \frac{\partial}{\partial z}(u\omega) = -\frac{Ra Pr}{A}\frac{\partial T_f}{\partial r_f} + Pr\left[A\frac{\partial}{\partial r_f}\left(\frac{1}{r_f}\frac{\partial}{\partial r_f}(r_f v)\right) + \frac{1}{A}\frac{\partial}{\partial z}\left(\frac{\partial \omega}{\partial z}\right)\right] \tag{3.18}$$

Its finite-difference form for the first half-time step is

$$C_{24}\omega^{k+\frac{1}{2}}_{i-1,j} + \left(\frac{2}{\Delta t} + C_{25}\right)\omega^{k+\frac{1}{2}}_{i,j} + C_{26}\omega^{k+\frac{1}{2}}_{i+1,j} = C_{27}\omega^{k}_{i,j-1} + \left(\frac{2}{\Delta t} + C_{28}\right)\omega^{k}_{i,j} + C_{29}\omega^{k}_{i,j+1} - C_{30}\left(T^{k+1}_{i,j+1} - T^{k+1}_{i,j-1}\right) \tag{5.34}$$

where the vorticity is expressed explicitly in the r direction but implicitly in the z direction. For the second half-time step, the vorticities are switched between their explicit and implicit expressions, giving

$$(-C_{27})\omega^{k+1}_{i,j-1} + (\frac{2}{\Delta t} - C_{29})\omega^{k+1}_{i,j} + (-C_{28})\omega^{k+1}_{i,j+1}$$

$$= (-C_{24})\omega^{k+\frac{1}{2}}_{i-1,j} + (\frac{2}{\Delta t} - C_{25})\omega^{k+\frac{1}{2}}_{i,j} + (-C_{26})\omega^{k+\frac{1}{2}}_{i+1,j} - C_{30}(T^{k+1}_{i,j+1} - T^{k+1}_{i,j-1}) \qquad (5.35)$$

where C_{24} through C_{30} have been defined in Table 5.1.

Since the driving force for buoyancy-driven flow in water is induced by the water temperature variation, the water energy equation must be solved prior to the solution of the vorticity transport equation. The temperatures of water solved from the energy equation are used in the vorticity transport equation, and these temperatures are kept constant for each 'full' time step in the iteration.

The vorticity boundary conditions have been given in Chapter IV as

$z = 0$

$$\omega_{i,j} = \frac{-2\psi_{i-1,j}}{Ar_j \Delta z^2_{i-1}} \qquad (4.23)$$

$z = 1$

$$\omega_{1,j} = \frac{-2\psi_{2,j}}{r_j \Delta z_1^2} \tag{4.24}$$

$r = 1$

$$\omega_{1,J} = \frac{-2\psi_{1,J-1}}{r_{J-\frac{1}{2}} \Delta z_{J-1}^2} \tag{4.25}$$

The boundary grid-point locations are shown in Figure 5.6. The three boundary conditions given above are for solid boundaries, at the centerline, the vorticity is zero because of equation (3.14), in which the terms V_r and $\partial V_z/\partial r$ both vanish.

In practice, with the exception of the known vorticity along the centerline, the vorticity values along the solid boundaries are unknown a priori, an iteration must therefore be used to find them. The approach used in this dissertation is (i) make a guess of the boundary vorticities, (ii) solve vorticities at all interior points in water using the vorticity transport equations (5.34) and (5.35), (iii) use the vorticities found in step (ii) in the stream function equation (3.19) to obtain new stream function values, and (iv) use these new stream function values in equations (4.23) to (4.25) to compute a refined set of boundary vorticities.

In order to safeguard the computed vorticities from converging to erroneous results, as warned by Israeli [53], the boundary vorticities computed using equations (4.23) to (4.25) are fine-tuned

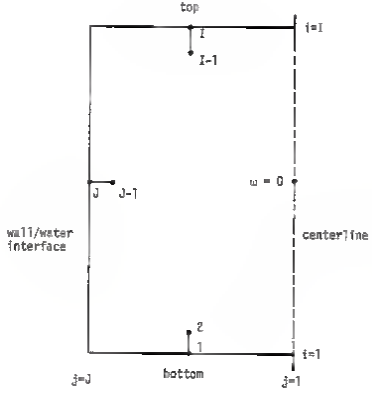

Figure 5.6 Water region vorticity boundary conditions

using the following formula

$$\omega_b^{l+1} = \omega_b^{l} + \kappa\psi_n^{l} \tag{5.36}$$

In this equation, ω_b^l refers to the boundary vorticities computed from equations (4.23) to (4.25), ψ_n stands for a finite-difference approximation to the normal derivative of the stream function evaluated at the boundary. The quantity κ represents an iteration parameter whose value is taken to be 0.5 in the present study. The superscripts l and l+1 are used to designate iteration index. Equation (5.36) enables computation of convergent boundary vorticities while inducing the no-slip condition that is necessary for any solid boundary.

In practice, the boundary vorticities at each half-time step are obtained by interpolating the old and new vorticity values as follows [54].

$$\omega_b^{l+\frac{1}{2}} = (\omega_b^{l} + \omega_b^{l+1})/2 \tag{5.37}$$

where ω_b^{l+1} refers to the vorticity calculated from equation (5.36). The convergence of the vorticities computed at each grid point is checked by using [55]

$$\underset{\text{boundary}}{\text{Max}} \left| \frac{\omega_b^{l+1} - \omega_b^{l}}{\omega_b^{l+1}} \right| \leq 10^{-3} \tag{5.38}$$

This convergence criterion will be reexamined in Chapter VII.

When the vorticity boundary conditions are incorporated into the finite-difference equations (5.34) and (5.35), the resulting equations can be expressed in a matrix form

$$\bar{\bar{A}}\,\bar{C} = \bar{B} \tag{5.39}$$

where matrix A and vectors B and C are defined differently for different time steps. For the first half-time step,

$$\bar{\bar{A}} = \begin{vmatrix} (\frac{2}{\Delta t} + C_{25})\ (C_{26}) & & & \\ (C_{24})\ (\frac{2}{\Delta t} + C_{25})\ (C_{25}) & \ddots & & \\ & \ddots & \ddots & \\ & & (C_{24})\ (\frac{2}{\Delta t} + C_{25})\ (C_{26}) & \\ & & & (C_{24})\ (\frac{2}{\Delta t} + C_{25}) \end{vmatrix} \tag{5.40a}$$

$\bar{J}$; j = 2,3,...,J-1

$$
\begin{vmatrix}
C_{27}\omega^{k}_{2,j-1}+(\frac{2}{\Delta t}+C_{28})\omega^{k}_{2,j}+C_{29}\omega^{k}_{2,j+1}-C_{30}(T^{k+1}_{2,j+1}-T^{k+1}_{2,j-1})-C_{24}\omega^{k+\frac{1}{2}}_{1,j} \\
C_{27}\omega^{k}_{3,j-1}+(\frac{2}{\Delta t}+C_{28})\omega^{k}_{3,j}+C_{29}\omega^{k}_{3,j+1}\ C_{30}(T^{k+1}_{3,j+1}-T^{k+1}_{3,j-1}) \\
\vdots \\
C_{27}\omega^{k}_{I-2,j-1}+(\frac{2}{\Delta t}+C_{28})\omega^{k}_{I-2,j}+C_{29}\omega^{k}_{I-2,j+1}-C_{30}(T^{k+1}_{I-2,j+1}-T^{k+1}_{I-2,j-1}) \\
C_{27}\omega^{k}_{I-1,j-1}+(\frac{2}{\Delta t}+C_{28})\omega^{k}_{I-1,j}+C_{29}\omega^{k}_{I-1,j+1}-C_{30}(T^{k+1}_{I-1,j+1}-T^{k+1}_{I-1,j-1}) \\
-C_{26}\omega^{k+\frac{1}{2}}_{1,j}
\end{vmatrix}
\tag{5.40b}
$$

$\bar{C}$; j = 2,3,...,J-1

$$
\begin{vmatrix}
\omega^{k+\frac{1}{2}}_{2,j} \\
\vdots \\
\omega^{k+\frac{1}{2}}_{I-1,j}
\end{vmatrix}
\tag{5.40c}
$$

At the second half-time step,

$$\bar{A} \; \begin{vmatrix} (\frac{2}{\Delta t} - C_{28}) & (-C_{29}) & & & \\ (-C_{27}) & (\frac{2}{\Delta t} - C_{28}) & (-C_{29}) & & \\ & \ddots & \ddots & \ddots & \\ & & (-C_{27}) & (\frac{2}{\Delta t} - C_{28}) & (-C_{29}) \\ & & & (-C_{27}) & (\frac{2}{\Delta t} - C_{28}) \end{vmatrix} \tag{5.41a}$$

$$\bar{B} \quad i = 2,3,\ldots,I-1$$

$$\begin{vmatrix} (-C_{24})\omega_{i-1,2}^{k+\frac{1}{2}} + (\frac{2}{\Delta t} - C_{25})\omega_{i,2}^{k+\frac{1}{2}} + (-C_{26})\omega_{i+1,2}^{k+\frac{1}{2}} - C_{30}(T_{i,3}^{k+1} - T_{i,1}^{k+1}) + C_{27}\omega_{i,1}^{k+1} \\ (-C_{24})\omega_{i-1,3}^{k+\frac{1}{2}} + (\frac{2}{\Delta t} - C_{25})\omega_{i,3}^{k+\frac{1}{2}} + (-C_{26})\omega_{i+1,3}^{k+\frac{1}{2}} - C_{30}(T_{i,4}^{k+1} - T_{i,2}^{k+1}) \\ \vdots \\ (-C_{24})\omega_{i-1,J-2}^{k+\frac{1}{2}} + (\frac{2}{\Delta t} - C_{25})\omega_{i,J-2}^{k+\frac{1}{2}} + (-C_{26})\omega_{i+1,J-2}^{k+\frac{1}{2}} - C_{30}(T_{i,J-1}^{k+1} - T_{i,J-3}^{k+1}) \\ (-C_{24})\omega_{i-1,J-1}^{k+\frac{1}{2}} + (\frac{2}{\Delta t} - C_{25})\omega_{i,J-1}^{k+\frac{1}{2}} + (-C_{26})\omega_{i+1,J-1}^{k+\frac{1}{2}} - C_{30}(T_{i,J}^{k+1} - T_{i,J-2}^{k+1}) \\ + C_{29}\omega_{i,J}^{k+1} \end{vmatrix} \tag{5.41b}$$

$\bar{C}$ — i = 2,3,...,i-1

$$\begin{vmatrix} \omega_{i,2}^{k+1} \\ \vdots \\ \omega_{i,j-1}^{k+1} \end{vmatrix} \tag{5.41c}$$

where C_{24} through C_{30} have been defined in Table 5.1. Once again, both A matrices are tridiagonal.

5.5 Finite-Difference Formulation for Stream Function Equation

The stream function equation has been given in Chapter III as

$$\frac{1}{Ar_f^2}\frac{\partial}{\partial z}\left(\frac{\partial \psi}{\partial z}\right) + A\frac{\partial}{\partial r_f}\left(\frac{1}{r_f}\frac{\partial \psi}{\partial r_f}\right) = -\omega \tag{3.19}$$

Since the solid boundaries and the centerline of the tank can be considered as one of the streamlines, a stream function value zero is chosen for this streamline. As has been mentioned in Chapter IV, this stream function equation (3.19) will be solved by using a successive-over-relaxation (SOR) method, as will now be shown.

The finite-difference approximation of equation (3.19) is

$$\left(\frac{C_{11}}{r_j} + \frac{C_{12}}{r_j} + AC_9 + AC_{10}\right)\psi_{i,j} = \frac{C_{12}}{r_j}\psi_{i+1,j} + \frac{C_{11}}{r_j}\psi_{i-1,j} + AC_9\psi_{i,j+1} + AC_{10}\psi_{i,j-1} + \psi_{i,j} \tag{5.42}$$

where C_9 through C_{12} have been defined in Table 5.1. The Gauss-Seidel iteration is used to write

$$\psi^{l+1}_{i,j} = \frac{\frac{C_{11}}{r_j}\psi^{l+1}_{i-1,j} + \frac{C_{12}}{r_j}\psi^{l}_{i+1,j} + AC_9\psi^{l}_{i,j+1} + AC_{10}\psi^{l+1}_{i,j-1} + \omega_{i,j}}{\frac{C_{11}}{r_j} + \frac{C_{12}}{r_j} + AC_9 + AC_{10}} \tag{5.43}$$

where the superscript l refers to the iteration index. The computed stream function value is over relaxed by using the formula

$$\psi^{l+1}_{i,j} = (1 - \lambda)\psi^{l}_{i,j} + \lambda\psi^{l+1}_{i,j} \tag{5.44}$$

where λ represents the relaxation factor and a value of 1.7 is tested for use in the present study. In the numerical computation carried out in this work, the stream function values at each grid point are computed repeatedly until these values converge and satisfy the following criterion

$$\underset{i,j}{\text{Max}} \left| \frac{\psi^{l+1}_{i,j} - \psi^{l}_{i,j}}{\psi^{l+1}_{i,j}} \right| \leq 10^{-4} \tag{5.45}$$

5.6 Solution Algorithm

To close this chapter, a solution algorithm is provided as follows:

(1) Use the temperature of the previous time step as an initial guess. (For the first time step, the initial temperature is used to initiate computation.)

(2) Compute a new set of temperatures at each grid point using equations (5.18) and (5.30).

(3) Check heat-flux continuity at wall/water interface by using equation (5.33). If this condition is not met, then modify the interface temperatures using equation (4.3) and return to step (2) above.

(4) Use the vorticities of the previous time step as an initial guess. (For the first time step, the vorticities are assumed to be zero everywhere to initiate computation.)

(5) Solve the vorticity transport equation (5.39) at interior grid points.

(6) Solve the stream function equation (5.44) using the new vorticities obtained in step (5) above.

(7) Compute new boundary vorticities using stream functions found in step (6) above. Check the convergence of boundary vorticities using equation (5.38). If the convergence criterion is not met, then modify the boundary vorticities using equation (5.36) and return to step (5) above.

(8) Calculate grid-point velocities using equations (4.22) and (4.26).

The procedure given above is for one (full) time step. The whole procedure is repeated for the next time step until the desired time is reached.

CHAPTER VI
RESULTS AND DISCUSSION

The enclosure under investigation has an aspect ratio 4, it measures 60 cm high and 15 cm radius. The enclosure wall is made up of 1% carbon steel and insulated with soft rubber, both being 0.4 cm thick. Thermophysical properties of these materials are given together with water in Appendix A. The initial (dimensionless) temperature distribution in water is given as shown in Figure 3.1, the initial temperature of the wall is unity throughout. The actual temperatures corresponding to the dimensionless temperatures 0.2 and 1.0 marked in the figure are 20°C and 60°C, respectively. The ambient air temperature is kept constant at 10°C.

In the numerical computation, a grid system of 41X21 points is used for the water. Grid systems of 41X10 or 41X6 are used respectively for the wall with, or without, insulation. A (full) time step used in the computation is 2 seconds. Selection of the grid size and time step is subjected to tests later (Chapter VII). The numerical results presented in this chapter were obtained using a Harris 800 computer and computed with double precision.

In order to view the flow and temperature fields in water, isotherms are plotted together with velocities and stream functions, see, for example, Figure 6.1. The spaces provided for velocities (middle figure in each set) are too small to plot vectors, only line

segments are thus shown. With the help of the stream function plots given on the right, the direction of the velocity can be identified. Specifically, a positive stream function value represents a counterclockwise circulation loop and vice versa. Both the velocities and stream functions plotted are normalized by their instantaneous maximum values found in the flow field. The thickness of the wall in the isotherm plot (left figure) is tripled in order to give a clear view of the isotherms.

6.1 Flow and Temperature Fields in Water for Different Designs of the Wall

Prior to the presentation of numerical results for comparing the flow and temperature fields resulting from wall design variations, physical mechanisms governing the flow and heat transfer are examined and given below.

(i) At the lower section of the tank where the wall temperature is initially higher than water, heat always transfers from the wall to the water during the early stage of cooling. At this time, since the convective resistance at the water side is always smaller than that at the air side, more heat tends to flow to the water from the wall.

(ii) Since the ambient air is always at a lower temperature, the wall will lose heat to the air once cooling starts. On the other hand, for the tanks under investigation, the water at the top section of the tank is always at a temperature higher than that at the bottom, heat will thus leak from the top to the bottom via the tank wall. This heat-leak problem is particularly pronounced for a tank

wall made up of a good thermal conductor. For such a wall, the physical mechanism leading to the heat leak is that the wall, being heated by the hot water above, is able to maintain a temperature that is slightly higher than the water at the same level, a convective loop thus forms at this level. As to how far this heat will penetrate downward along the wall depends greatly on the effectiveness of heat transfer in the wall as well as the amount of heat that is simultaneously lost by convection from the wall to the outside air. The difference between these two controls the heat penetration length.

6.1.1 Uninsulated Tank

For the ease of reference later, this case of tank wall without insulation on it will be called NI for short. For this case, because of the physical mechanism (1) described above, clockwise circulation loops form in the lower section of the tank, see Figure 6.1(a). The wall being highly conductive, the temperature gradient across the wall is negligibly small, a situation contributing to the horizontal isotherms viewed in this region.

For this NI case at 180 seconds, the temperature of the lower wall drops to a level where the lower circulation loops in water start to weaken. In the mean time, the top wall cools down due to heat loss to the ambient air, circulation loops thus form in this top region. These top and bottom loops move in opposite direction as revealed by the stream function values marked.

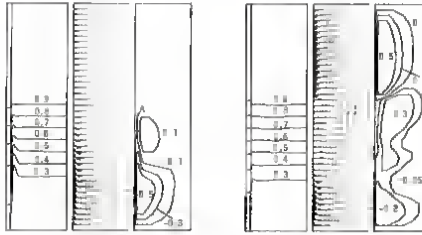

(a) 60 seconds (b) 180 seconds

Figure 6.1 Isotherm- velocity field and streamline for tank without insulation

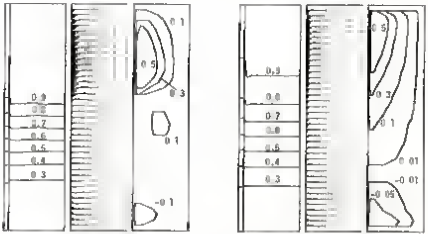

(c) 300 seconds

(d) 3600 seconds

Figure 6.4—continued

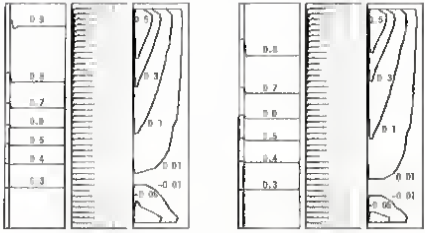

(e) 7200 seconds

(f) 10800 seconds

Figure B-1 continued

A short while later at 300 seconds, the lower circulation loops nearly disappear, the top circulation loops, however, still persist. In fact, because of the continuous heat loss from the wall, the upper circulation loops intensify and are now able to penetrate deeper and deeper into the lower region, see Figures 6.1(d), (e), and (f). A quasi-steady state is finally reached, and the stratification of water in the tank is also destroyed as shown by the isotherm locations plotted, also see the centerline water temperatures plotted in Figure 6.2.

6.1.2 Tank Insulated from the Outside

Placing insulation over the outside of the wall (referred to later as EI case for short) increases the initial heat transfer from the wall to water. As expected, the heat loss from the wall to the ambient air is now reduced, as a result, the upper circulation loops cannot develop as rapidly as in the previous NI case, compare Figures 6.1(b) and 6.3(b). The heat leak via the conductive wall, however, becomes more serious, see the circulation loops plotted in the lower section of the tank at 300 seconds, Figure 6.3(c). A comparison of the isotherm locations also indicates that the stratification in water decays more rapidly in this case. The centerline water temperatures given in Figure 6.4 also serve to illustrate this point.

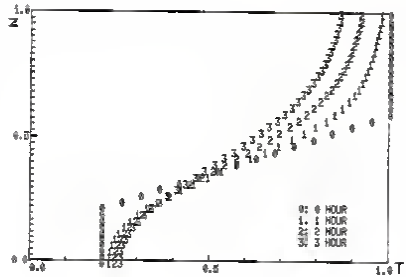

Figure 5.2 Centerline water temperature variation with time for tank without insulation

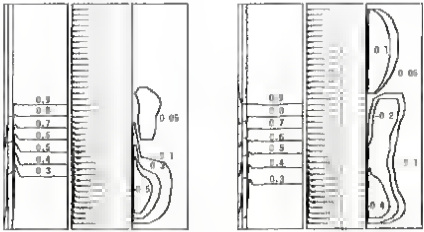

(a) 60 seconds

(b) 180 seconds

Figure 5-3 Isotherm velocity field- and streamline for tank with exterior insulation

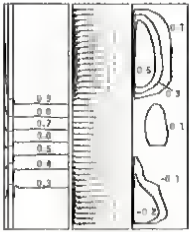

(c) 300 seconds

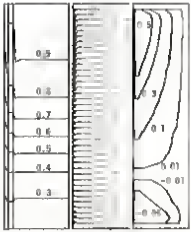

(d) 3600 seconds

Figure 5.3 continued

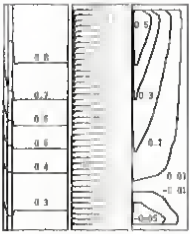

(e) 7200 seconds

(f) 10800 seconds

Figure 6.3-continued

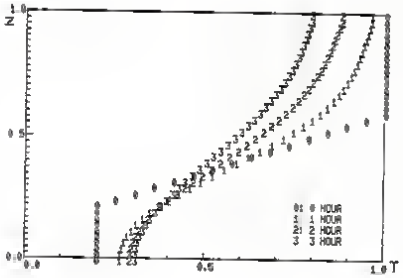

Figure 6.4 Centerline water temperature variation with time for tank with exterior insulation

6.1.3 Tank Insulated at the Inside

For a tank wall insulated at the inside (II case), the heat leak from the hot water to the cold water is inhibited because of the insulation. This reduction of heat leak results in smaller circulation loops both at the top and bottom sections of the tank, see Figure 6.5. At very long time (3,600 seconds), small counterclockwise loops also develop at the bottom section of the tank, a result of the heat loss from the lower wall to the ambient air. Stratification in water is well preserved in this case, as demonstrated by the isotherms plotted in Figure 6.5 as well as the centerline water temperatures shown in Figure 6.6

6.2 Heat Fluxes at Wall/Water Interface

An attempt is also made to calculate the heat flux along the wall/water interface. Fourier's law, in finite-difference form, is used to evaluate the heat flux at the water side, and the results are plotted in Figures 6.7 through 6.9. In these figures, a positive heat flux value stands for a heat flow from water to wall and vice versa. The z coordinate is dimensionless, while the heat flux is dimensioned.

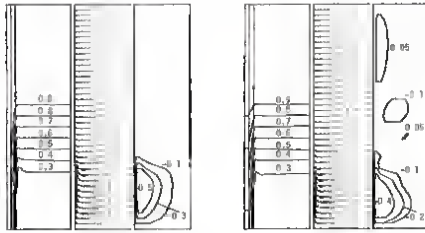

(a) 80 seconds

(b) 180 seconds

Figure 6 5 Isotherms, velocity field and streamline for tank with interior insulation

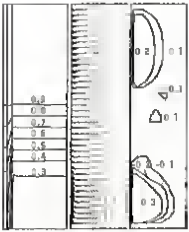

(c) 300 seconds

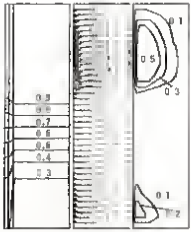

(d) 600 seconds

Figure 8.5-continued

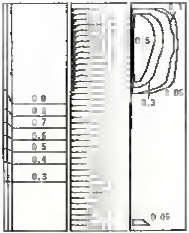

(e) 1200 seconds

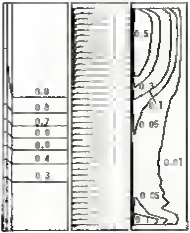

(f) 3600 seconds

Figure 8 S-continued

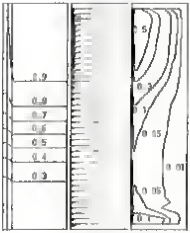

(a) 2800 seconds

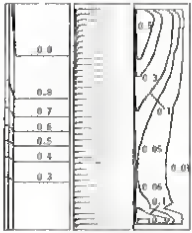

(b) 19800 seconds

Figure 8 5-continued.

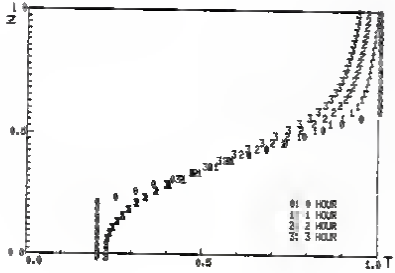

Figure 6.6 Centerline water temperature variation with time for tank with interior insulation

6.2.1 Heat Flux Distribution for N1 Case

The observations made in section 6.1 relating to velocity and temperature fields can be supported by the heat flnxes presented in this section. Take the N1 case at 60 seconds (Fig. 6.7) for example. Heat flows from the wall to water in the lower section of the tank, in the top section, the heat flnx direction is reversed. For longer times at 180 and 300 seconds, the lower heat fluxes diminish rapidly. There are points at about z = 0.2 and 0.6 where the heat flnxes reach their maximum values. This may be ellnded to the heat penetration length discussed in section 6.1. The heat transfer in the tank wall is complicated because, on one hand, the wall receives heat from the hot water above, while on the other hand, the well also dissipetes the heat thet it receives to the ambient eir. The problem is further complicated by the fect that, at the water side, the temperature is stratified.

For times past 300 seconds, heet loss from the water comes mainly from the top. The heat flux curves plotted in Figure 6.7(b) serve well to illustrate this point.

6.2.2 Heat Flux Distribution for E1 Case

For a tank wall insulated from the outside, the heet transfer from the lower wall to water is increased, note the scale change for q in Figure 6.8. The heet loss from the top section of the wall is reduced because of the insuletion.

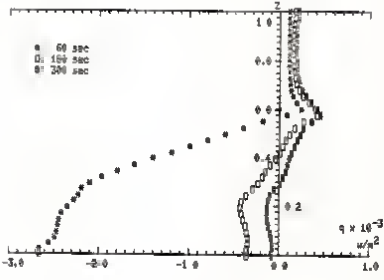

(a)

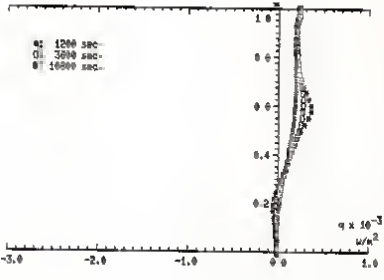

(b)

Figure 6.7 Heat flux distribution for tank without insulation

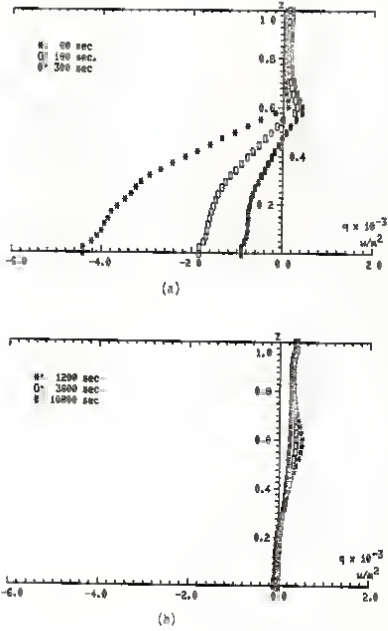

Figure 6.8 Heat flux distribution for tank with exterior insulation

e.2.3 Heat Flux Distribution for II Case

For e tank wall insulated et the inside, the heet loss from the top section of the tank is the lowest of the three cases studied, see Figure 6.8.

To facilitate comparison of the heet fluxes coeputed for the three cases above, e composite diegram is constructed as shown in Figure 6.10. A change in scale for q should be noted for Figures 6.10(h) and (c).

6 3 Convective Coefficients et the Air Side

The convective heat loss free the wall et the eir side can be evaluated by using equation (4.5). Newton's cooling lew can be used together with this equation to find the local convective coefficient as plotted in Figure 6.11. It is difficult to precisely pinpoint why the convective coefficient varies as plotted beceuse, from equation (4.5), the local heat flux free a nonisothermal weil is e complicated function of the local teeperature excess over the ambieet tampereture, and the gradient of this teeperature excess elong the wall, among others. Some basic feetures can nevertheless be feund free these curves as described beiow.

For all the three cases studied, the convective coefficient is elways the largest neer the bottam end of the well, a result of the small beundary-leyer thickness there. This coefficient drops off rapidly as it maves up elang the wall. The veriation of the convective coefficient is somewhet irregular et higher elevations, however, the magnitude of tnis coefficient is still reesenable.

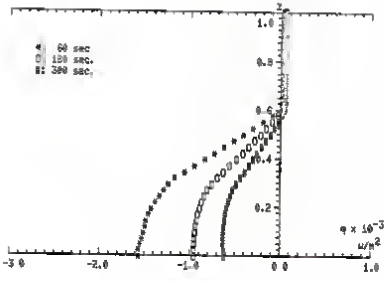

(a)

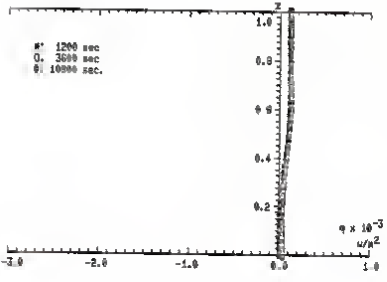

(b)

Figure 6.8 Heat flux distribution for tank with interior insulation

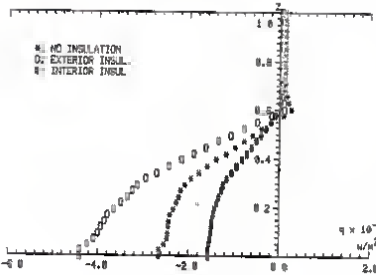

(a) 60 seconds

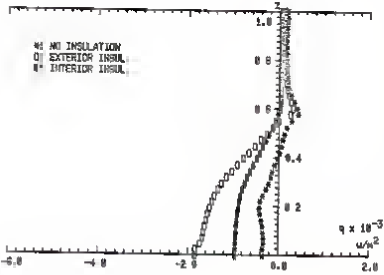

(b) 180 seconds

Figure 6.10 Heat flux distribution for three designs of the wall at different times

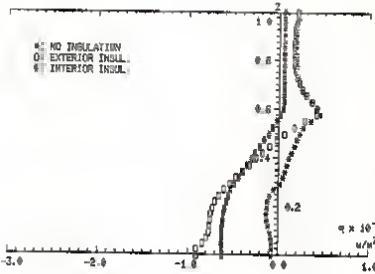

(c) 300 seconds

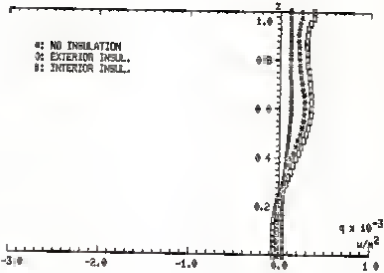

(d) 3600 seconds

Figure 5.10-continued.

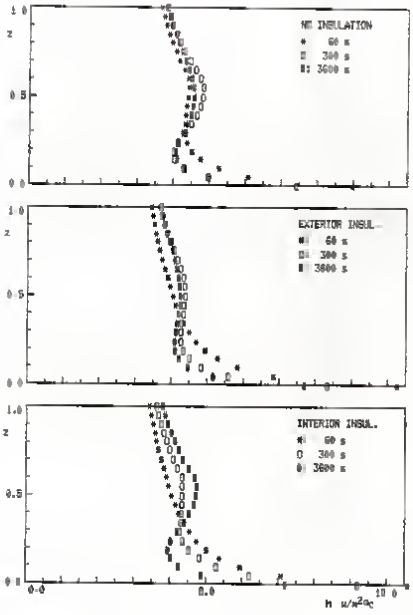

Figure 6.11 Heat transfer coefficients for three designs of the wall

For all the cases tested, the convective coefficient varies from 3.5 to 5 $w/m^2°C$.

6.4 Velocity and Temperature Distributions in the Boundary Region

The velocity and temperature profiles in the boundary region at time equal to 60 seconds are plotted in Figures 6.12 and 6.13. The elevation z and the radial position r in these plots are dimensionless, whereas the axial velocity is dimensioned. The dimensionless temperature plotted is measured in excess of that temperature measured at the centerline and at the same elevation. Some trends can be seen from these curves.

As shown in Figure 6-12, of the three cases studied, the E1 case always has the largest velocity in the boundary layer, the velocity for the I1 case is the smallest. Similarly, in the temperature plots given in Figure 6.13, the dimensionless water temperature is always the largest for the E1 case and the smallest for the I1 case. Because of the short time (60 seconds) chosen for these plots, the lower half of the wall is always at a temperature higher than water, the velocities of water in the boundary region are thus positive close to the wall.

It is informative to examine the magnitude of the water velocity in the boundary region. The maximum axial velocity of water calculated for E1 case is 0.38 cm/s. Also, the thickness of the velocity boundary layer where the flow velocity is positive accounts for about 5 to 10% of the tank radius. These magnitudes appear to be in reasonable agreement with the experimental data reported by

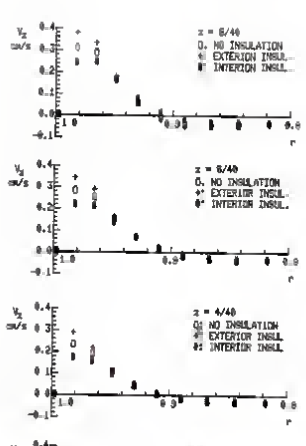

Figure 6.12 Velocity profiles at various elevations at 60 seconds for three designs of the wall

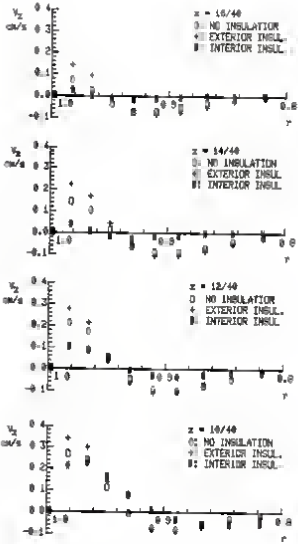

Figure 6.12-continued.

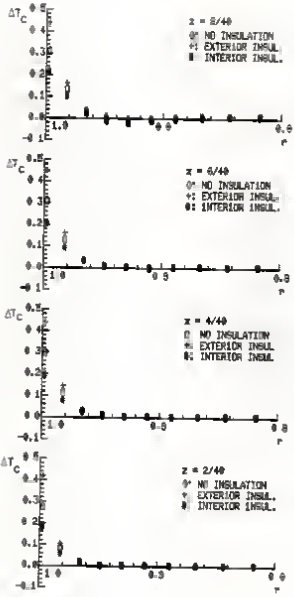

Figure 6.13 Temperature profiles at various elevations at 60 seconds for three designs of the wall

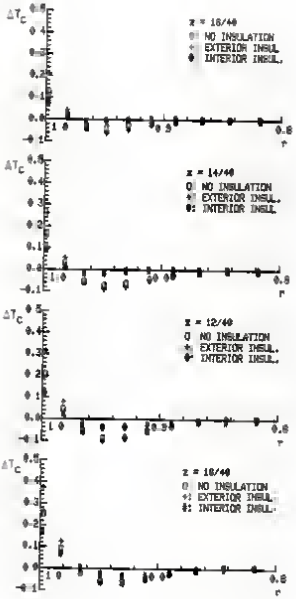

Figure 6.13-continued

Hess and Millar [18] who used a laser Doppler velocimeter to measure the water velocity near the wall in the cold region of a thermocline. This region corresponds to the lower section of the tank in the present study, use of their data for comparison in Table 6.1 is thus justified.

A close examination of the velocity plots given in Figure 6.12 reveals that, for tank elevations above about H/40, the velocity profiles consist of two branches: an upward-pointed velocity region close to the wall, and a downward-pointed velocity region away from the wall. The temperature profiles given in Figure 6.13 can be divided in a similar fashion, the dimensionless temperature close to the wall is positive, while this temperature away from the wall is negative. These peculiar velocity and temperature distributions are commonly referred to as flow reversal and temperature defect, respectively, as will now be discussed.

6.5 Flow Reversal and Temperature Defect

A detailed study of the flow reversal and temperature defect requires a close examination of the flow field in the lower section of the tank. Take the N1 case for example, an enlarged view of the flow field near the wall up to an elevation of grid line 21 is given in Figure 6.14. The directions of the line segments, representing velocities, are slowly turning in the region away from the wall. To support this observation, the velocities at two elevations (i = 13 and 11) are replotted as shown in Figure 6.15, in which each velocity vector is decomposed into its z and r components. At a lower

Table 6.I Comparison between numerical and experimental data

	Experiment*	Present study**
Axial velocity inside the boundary layer	0.45 cm/s (maximum) 0.25 cm/s (typical)	0.38 cm/s (maximum) 0.02 ~ 0.38 cm/s
Core axial velocity	0.01 cm/s (typical)	0.005 ~ 0.056 cm/s
Boundary layer thickness	5 ~ 10% of radius	5 ~ 10% of radius

* Data [18] given are for observations made within the first 3 minutes of the experiment for EI case

** EI case at 60 seconds

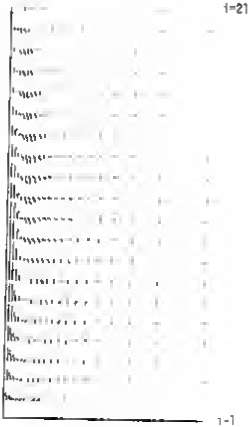

Figure 6.14 An enlarged view of the flow field in the lower section of the enclosure in Fig. 6.1(a)

(a) i=13 grid line

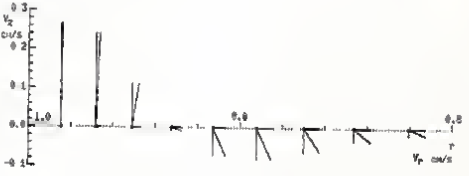

(b) i=11 grid line

Figure 6.15 Decomposition of velocity vectors into their z and r components

elevation of l = 11, the r-component velocities increase with decreasing r (moving away from the wall), contributing to a rapid rotation of the velocities at this elevation. This velocity rotation and eventual reversal are largely responsible for the wedge-like streamlines viewed at point A in Figure 6.1(e). As expected, the radial component of the velocity causes flow recirculation, the z-component velocity gives rise to a flow reversal.

Study of flow reversal and temperature defect is facilitated by simultaneously viewing the velocity and temperature profiles plotted for this elevation (l = 11) in Figure 6.16. Comparing the radial positions for these profiles enables one to see that the region where there is a temperature defect (negative temperatures) does not correspond exactly to the region where there is a flow reversal (negative velocities) [56,57]. The point where the velocity curve crosses over from positive to negative is located farther away from the wall.

The physical mechanism leading to this temperature defect and flow reversal will now be examined, and a short note is in order to explain how the velocity boundary layer is formed for a buoyancy-driven flow [58]. Refer to the two figures shown in Figure 6.17. In the lower figure, the total thickness of the velocity boundary layer can be divided into two parts. The one close to the wall is a heated layer where the dimensionless temperature is positive, this is the region where the velocity distribution is a result of balance of buoyancy force and friction force. Moving away from the wall, there is an unheated layer where the dimensionless temperature is zero, the

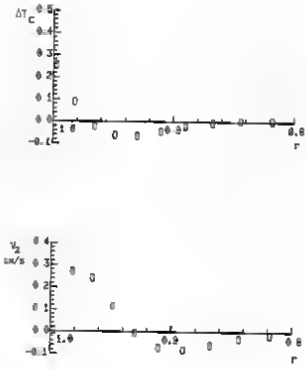

Figure 8-15 Temperature and velocity profiles for NI case at i = 11 grid line

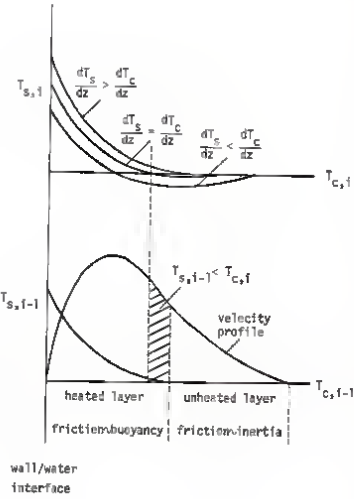

Figure 6.17 Boundary layers on a vertical, heated surface

formation of the velocity in this layer is the balance of frictian force and inertia force.

Notice that for the buoyancy-driven flow of interest in this study, the water moves in a stratified medium in which the wall temperature is not uniform. Then, several changes may occur when the water moves up to a new environment. Refer to the top figure in Figure 6.17, which is a plot of the water temperature at a higher elevation. If the temperature gradient along the wall in the z direction is greater than that gradient of water along the centerline, that is $dT_s/dz > dT_c/dz$, then the thermal boundary layer thickness will grow. Otherwise, temperature defect will occur. Physically, one may say that there must be sufficient temperature rise in the wall in the direction of flow in order for water to sustain a growing thermal boundary-layer thickness, an insufficient temperature rise in the wall will result in the local water temperature being lower than the ambient water at the same elevation, thus causing temperature defect [59-63].

In order to determine the temperature defect region for time equal to 60 seconds, the temperature gradients of the wall and water are plotted versus z as shown in Figure 6.18. The region where $dT_c/dz > dT_s/dz$ is marked for temperature defect.

The mechanism causing flow reversal can now be explained by again referring to Figure 6.17. In the top figure, the r position where there is temperature defect can be considered a region of negative buoyancy force. This region is in the unheated layer in the velocity profile (lower figure) where the water velocity is mainly a

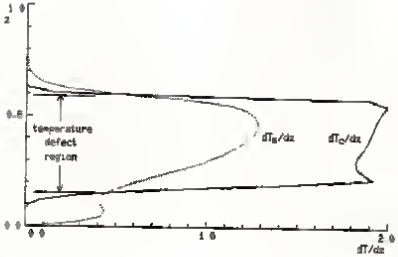

Figure 6.18 Determination of temperature defect region by comparing two temperature gradients

result of inertia and friction forces. Then, for water coming from below that is in the outer part of the velocity boundary layer, a negative force will arise if the inertia force in water is unable to overcome the negative buoyancy force above. The direction of flow will reverse, thus causing flow reversal.

The fact that the crossover point of the velocity profile is located farther away from the wall than that of the temperature profile can also be explained, see Figure 6.13. Postulating that the entire velocity profile is the superposition of two profiles, one being the result of the positive branch of the temperature profile in δ_{T1}, and the other being the result of the temperature defect in δ_{T2}, then the superimposed velocity profile will look like the one shown in solid curve in Figure 6.13(b). The crossover location for the velocity profile is farther away from the wall because of the velocity in the positive branch being larger.

6.6 Energy Analysis

From the thermodynamic point of view, the cooling of water in tank should satisfy the energy conservation principle. The initial energy of wall and water should be equal to the energy of the wall and water at any moment corrected for that portion of heat that is lost from the wall to the ambient air. This latter heat correction should be integrated over time up to that moment for energy-loss analysis.

The energy analysis mentioned here serves two purposes. It provides a check of the accuracy of the numerical results (other

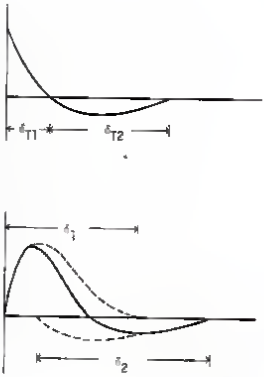

Figure 6.19 Superposition of two sections of temperature profile in (a) to obtain velocity profiles in (b)

checks will be given in the next chapter). It also enables a comparison of the capability of the tank in preserving the energy stored in water.

A plot of the difference between the initial total system energy and the total system energy at time t (with loss adjusted), normalized by the initial energy, is given in Figure 6.20. In this plot, a total satisfaction of the conservation principle by numerical results would require that this difference be zero at all times. For the three cases studied here, this energy conservation error ranges from -2 to 7% at three hours. Considering that it takes 5,400 full time-steps to reach three hours, and within each time-step many iterations are needed for computing convergent temperature, vorticity, and stream function values, plus the fact that there are approximations made in treating heat-flux continuities at interfaces, the numerical errors presented here appear reasonable.

A comparison of the ability of the tank in preserving energy is made in Figure 6.21. Here the ordinate is a ratio of the energy in water to its initial energy, and time is plotted along the x axis. For all three cases studied, there is an initial rise of energy in water due to heat transfer from the lower wall. All three curves drop off with time because of heat loss. Of the three cases tested, the E1 case is only slightly better than I1 case in preserving energy. However, in Section 6.1.2, it has been mentioned that stratification in water cannot be effectively preserved for this E1 case.

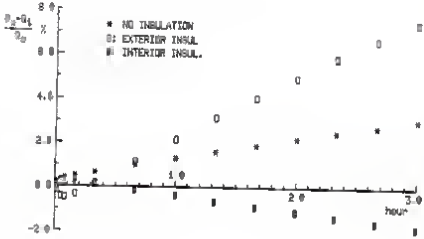

Figure 6.20 Numerical errors evaluated for three cases based on the energy conservation principle

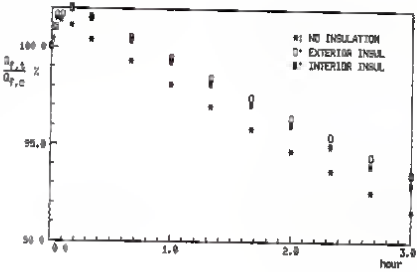

Figure 6.21 Comparisen ef ability of walls to preserve energy in water

6.7 Evaluation of Stratification Index

Thermal stretification is well preserved for case II. As a means for further demonstration of this important result, Figure 6.22 is given for the centerline water temperatures at 3 hours for three cases. The II case clearly stands out as being superior.

A stratification index is proposed as follows to evaluate the performance of storage tank in preserving stretification in a storage medium:

$$S_t = \frac{\overline{\left(\frac{dT}{dz}\right)_c}_t}{\overline{\left(\frac{dT}{dz}\right)_c}_0} \qquad (6.I)$$

here $\overline{(dT_c/dz)}_0$ is the mean temperature gradient in the stratified storage medium initially at the centerline of the tank. The differential in the numerator stands for the same temperature gradient at time t. Based on this definition, a perfectly stretified tank should have a S_t value unity at all times, and a good tank is one that has a high S_t value. For the three cases studied here, the values of S_t very from 0.35 for EI, 0.46 for NI, and 0.64 for II case at three hours. The ability of the interior insuletion to preserva thermal stratification is now verified quantitatively.

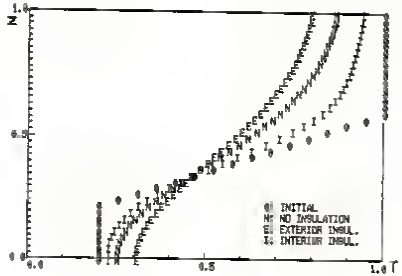

Figure 6.22 Centerline water temperature profiles at 3 hours for three designs of the wall

CHAPTER VII
REMARKS ON NUMERICAL RESULTS

Numerical solution of a physical problem is incomplete without test of convergence. A test of numerical results in satisfaction of the energy conservation principle has been given in Chapter VI. Other tests must be made to show that the numerical schemes are stable and the numerical results are convergent, and these are the tests that will be made here.

Tests of stability and convergence in this chapter will be made by varying the grid and time-step sizes in the computation. In the course of tests consideration will also be given to the computer (CPU) time used in the computation.

7.1 Effect of Time-Step Size on Stability and Convergence

Although the ADI method used in the solution of the vorticity transport and wall and water energy equations has been considered to be unconditionally stable according to the Fourier or von Neumann analysis, instability may still arise if boundary vorticity does not converge [52]. Bontoux et al. [64] made an extension of the Fourier stability analysis to study the effect of boundary conditions on the stability of the ADI method. They proposed a criterion for time-step limitation

$$\frac{\Delta t_c}{\Delta x^2} = \frac{1 + (1 + 2\beta/Pr)^{\frac{1}{2}}}{4} \qquad (7.1)$$

where both Δt_c and Δx are dimensionless. Notice that this equation was derived based on the analysis of natural convection in a differentially heated solar collector, which is, strictly speaking, not the kind of system being analyzed here, however, because of the solution methods used in their analysis being similar to the ones used in the present investigation, the criterion given above can, at least, be served as reference for selecting time-steps for tests.

The Prandtl number for water is taken to be 4.52 (value at 38°C), and equation (7.1) is used to compute

$$\frac{\Delta t_c}{\Delta x^2} = 0.263 \qquad (7.2)$$

For the 41X21 grid system used in the present investigation, the smallest grid size in water can be found to be 0.0156. Using this grid size in equation (7.2) yields a time-step that is equivalent to a real time of 36.5 seconds. The same criterion is applied to the wall, where, for a 41X6 grid system, the grid size, calculated based on the tank radius, is 0.00533. This yields a real time-step for the wall to be 4.27 seconds. This latter time-step being smaller is taken to be a reference for selecting test time-steps.

Several time-step sizes (1.0, 2.0, 3.0 and 4.0 seconds) are tested, and the results are plotted in Figure 7.1. In Figure 7.1(a), the number of iterations for computing convergent heat fluxes at

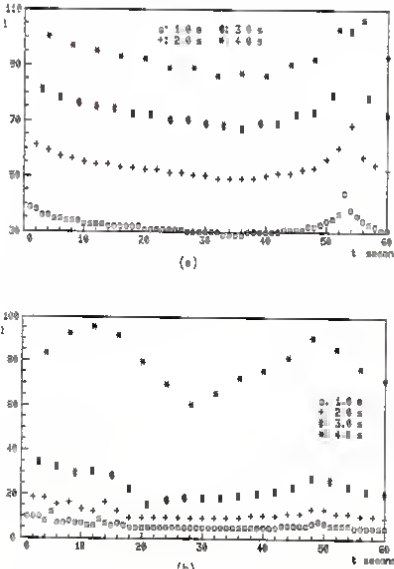

Figure 7.1 Iteration counts for convergence tests (a) heat flux, (b) boundary vorticity

wall/water interface is plotted versus cooling time of the tank. It is clear that the number of iterations increases rapidly with the time-step size. The same trend is found when computing convergent boundary vorticities, see Figure 7.1(b). Here the number of iterations for a time-step of 4 seconds starts to oscillate, and an increase of time-step to 5 seconds does not yield convergent results, indicating that the numerical stability limit for the time-step has been exceeded.

Since it is always desirable, if possible, to use a large time-step in order to reduce the number of steps computed, it is not clear whether such a practice is economical here because the number of iterations is also increased when the time-step size is increased. A comparison of CPU time is thus made as shown in Table 7.1. For the problem under investigation, a choice of 2 seconds time-step consumes the least computer time.

The fluid velocities are also tested for convergence at selected locations and the results are presented in Figure 7.2. For the four time-steps tested, numerical results for three time-steps of 1.0, 2.0, and 3.0 seconds are in close agreement at all elevations and radial positions tested, giving indication that the numerical results have converged at 2 seconds. This time-step has thus been used for computing all numerical results presented in Chapter VI.

7.2 Effect of Grid Size on Convergence

In the series of tests made above, the grid system employed in water was a 41X21-point system. For such a system, the velocities

Table 7.1 CPU time consumed for different time steps calculated up to 60 seconds' cooling time

time-step (second)	CPU time
1.0	1 h 4 min 8 s
2.0	57 min 36 s
3.0	1 h 13 min 19 s
4.0	2 h 33 min 34 s

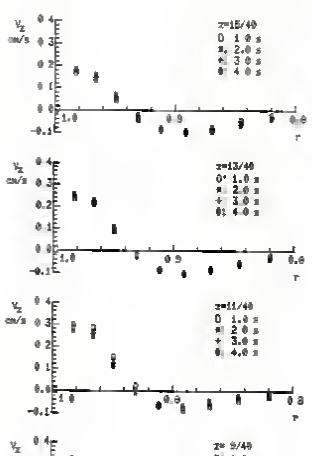

Figure 7.2 Axial velocity profiles for various time-steps at 60 seconds

have shown to converge for a time-step of 2 seconds, the numerical computation is also stable for this time-step, while the computer program is economical to run. It remains to be shown that this grid system is, in itself, good enough for a convergent solution.

The time-step used is still taken to be 2 seconds, and one additional grid system (61X21) is tested by analyzing their flow and temperature fields in water, and the results are plotted in Figure 7.3. A comparison of the streamlines for two grid systems shows that a 41X21 grid is already able to reveal much of the flow details. On the other hand, the z component velocities for the 41X21 system have also converged, see Figure 7.4. A change of grid system to 61X21 points in water, however, increases CPU time by a factor of 1.8 for 60 seconds' cooling time, an increase of grid points to 61X21 is thus unnecessary for the present investigation.

A test with 41X31 grid system was also attempted, and it takes about 40 hours CPU time to simulate 60 seconds' cooling time of the tank because of the excessive iterations needed. A prolonged simulation using this grid system was not made.

7.3 Test of Convergence Criteria for Vorticities

It is also desirable to check if the convergence criterion for boundary velocities in equation (5.38) is small enough to give accurate results. The z-component velocities are thus computed for a 41X21 grid system with two-second time-step and three convergence criteria of 10^{-3}, 10^{-4}, and 10^{-5}. As shown in Figure 7.5, the

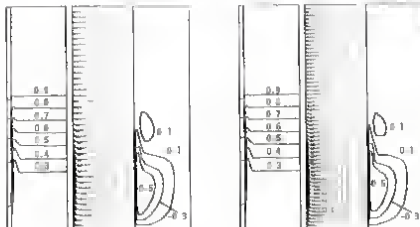

Figure 7.3 Isotherm velocity field and streamline for different grid systems at 60 seconds

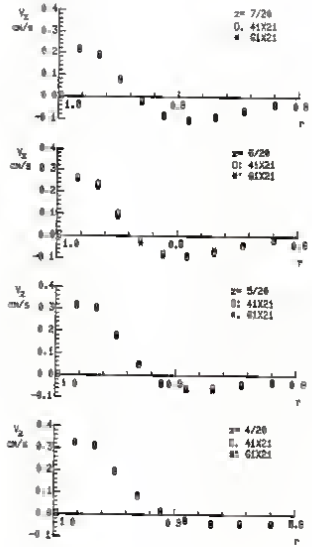

Figure 7.4 Axial velocity profiles for different grid systems at 60 seconds

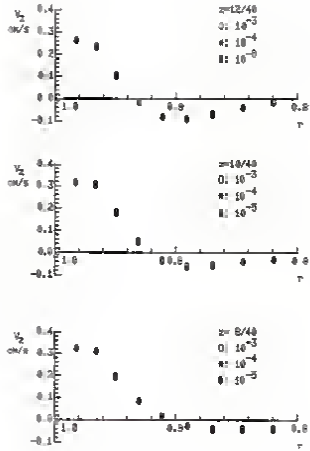

Figure 7.5 Axial velocity profiles for three convergence criteria of the boundary vorticity

velocities have converged for the 10^{-3} criterion used in the present investigation.

CHAPTER VIII
CONCLUSIONS AND RECOMMENDATIONS

A numerical study is presented for investigating unsteady natural convection in a stratified storage tank. Two different designs of tank wall are analyzed, one placing insulation on the outside of the wall, the other placing the insulation over the inside of the wall. An uninsulated tank is also studied for use as control. For all the cases studied, water is stratified at the midsection of the tank, hot water occupies nearly one third at the top section of the tank, while cold water is located at the bottom section. The wall temperature is initially uniform at the hot-water temperature level.

In the numerical solution, the wall and the water are treated as two separate regions, and conditions are derived for matching temperatures and heat fluxes at the wall/water interface. External heat convection from the wall to the ambient air is not treated as a separate region, but accounted for in the boundary conditions of the wall. The entire problem is solved as a conjugate heat transfer problem to determine the flow and temperature fields in water and the temperature field in wall.

In the solution, the governing equations are transformed into a vorticity-stream function formulation. Control-volume approach is used to derive finite-difference equations. Kinematically consistent

velocity fields are used to compute vorticities and stream functions, and a nonuniform grid system is employed to analyze the flow and temperature fields in water.

The wall and water energy equations and vorticity transport equation are solved by use of the ADI method, while the stream function equation is solved by use of the SOR method. The wall and water temperatures are computed simultaneously using the energy equations, while heat fluxes are checked at the wall/water interface to assure their continuity. The vorticity transport equation is solved together with the stream function equation, and the convergence of vorticity is checked by evaluating boundary vorticities. Two sequences of interations are used for each full-time step, and a total of 5,400 full-time steps are calculated for a real time of three hours' cooling of the tank.

The performance of each storage tank is evaluated on the basis of its isotherm, velocity, and stream function data. Test results indicate that both exterior and interior insulation are about equal in preserving energy, however, the interior insulation performs far better in retaining stratification in water. Based on the stratification index proposed in this dissertation, the interior insulation has an index value that is 85% higher than that of the exterior insulation. The merit of interior insulation is thus quantitatively established.

The velocity and temperature in the boundary layer at the early stage of cooling are also used to study flow reversal and temperature defect. The physical mechanisms leading to these phenomena are

given. The study is concluded with a series of tests in which the time step used in the computation is shown to be numerically stable. The grid size chosen for analysis and the convergence criterion selected for vorticity computation are both adequate in yielding convergent velocities in the boundary layer.

Based on the conclusions made above, some follow-up studies may be proposed as follows.

(1) The study made here is based on one aspect ratio. It is desirable to test other aspect ratios so that an optimum configuration of the tank may be determined.

(2) In the present study, the performance of the tank is analyzed under a static condition. It may be necessary to evaluate the performance of the tank under a dynamic condition.

(3) The numerical study presented here can be made more useful if it is verified by experiment. A limited experimental program serves well to meet this need. Once verified to be accurate, the computer program developed here can be used to test other operating conditions, thereby leading to an optimum use of the storage tank.

APPENDIX A
PHYSICAL PROPERTIES

	water (38°C)	air (10°C)	1% carbon steel	soft rubber
specific heat C_p, KJ/Kg°C	4.187		0.473	1.884
density ρ, Kg/m^3	993.1		7800	1110
conductivity k, w/m°C	0.63	0.025	43.0	0.173
coefficient of expansion β, K^{-1}	$3.6X10^{-4}$	$3.53X10^{-3}$		
kinematic viscosity ν, m^2/s	$6.87X10^{-7}$	$1.36X10^{-5}$		
diffusivity α, m^2/s	$1.576X10^{-7}$		$1.16X10^{-5}$	$8.27X10^{-8}$
Prandtl number Pr	4.52	0.714		

APPENDIX B
TIME SCALE ANALYSIS FOR DETERMINING HEAT TRANSFER MECHANISMS

The time-scale analysis given in this Appendix provides a qualitative prediction of the preferred heat transfer mechanisms in a storage tank. Such an analysis has also been made by others [58,65,66] to study other natural convection problems.

Consider the energy equation in the tank wall

$$\frac{\partial T_s}{\partial t} = \alpha_s\left(\frac{\partial^2 T_s}{\partial r^2} + \frac{1}{r}\frac{\partial T_s}{\partial r} + \frac{\partial^2 T_s}{\partial z^2}\right) \tag{3.24}$$

and the energy equation in the water medium

$$\frac{\partial T_f}{\partial t} + V_r\frac{\partial T_f}{\partial r} + V_z\frac{\partial T_f}{\partial z} = \alpha_f\left(\frac{\partial^2 T_f}{\partial r^2} + \frac{1}{r}\frac{\partial T_f}{\partial r} + \frac{\partial^2 T_f}{\partial z^2}\right) \tag{3.12}$$

Six time scales can be derived from these two equations and these time scales can be used to relate six heat transfer mechanisms as illustrated in Figure B.1. These time scales are defined as follows

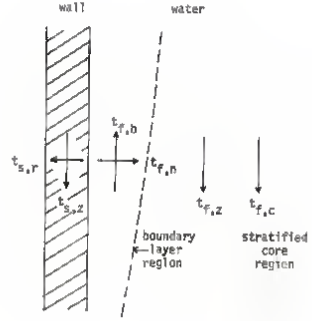

Figure 8.1 Six time scales for six heat-transfer mechanisms

$t_{s,z}$ time scale for z-direction heat conduction in the wall,

$t_{s,r}$ time scale for r-direction heat conduction in the wall,

$t_{f,n}$ time scale for r-direction heat conduction across the boundary layer,

$t_{f,b}$ time scale for z-direction heat convection in the boundary layer,

$t_{f,z}$ time scale for z-direction heat diffusion in the core region,

$t_{f,c}$ time scale for z-direction heat convection in the core region,

An order-of-magnitude analysis can be used to derive the expressions for time scales as follows.

(1) $t_{s,z}$

Consider the energy equation (3.24) for heat conduction in the z direction. Dropping the radial differential terms in this equation gives

$$\frac{\Delta T}{t_{s,z}} \sim a_s \frac{\Delta T}{(F_s H)^2} \tag{B.1}$$

where $F_s H$ is the fraction of the height of the wall along which there is a large temperature gradient. H is the height of this wall. This equation can be rearranged to be

$$t_{s,z} = \frac{F_s^2 H^2}{e_s} \tag{B.2}$$

A schematic diagram showing the wall length over which the temperature change is ΔT is provided in Figure B.2(a).

(ii) $t_{s,r}$:

Consider equation (3.24) in the r direction. Dropping the z differential term in this equation gives

$$\frac{\Delta T}{t_{s,r}} = e_s\left(\frac{\Delta T}{\delta^2} + \frac{1}{R_1}\frac{\Delta T}{\delta}\right) \tag{B.3}$$

Since $R_1 >> \delta$, the second term in the parenthesis is small. It follows that

$$t_{s,r} = \frac{\delta^2}{e_s} \tag{B.4}$$

The temperature gradient in the radial direction in the wall is shown schematically in Figure B.2(b).

(iii) $t_{f,n}$:

For heat transfer across the boundary layer, δ_T, the temperature drop across this layer is ΔT; see Figure B.2(c). Dropping the convection terms and the z-direction conduction term in equation

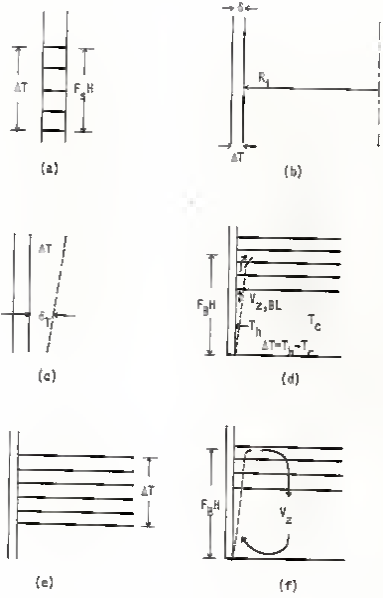

Figure 8.2 Schematic diagrams for studying time scales

(3.12) gives

$$\frac{\Delta T}{t_{f,n}} \sim \alpha_f \left(\frac{\Delta T}{\frac{\delta_T}{2}} + \frac{1}{R_f}\frac{\Delta T}{\delta_T}\right) \tag{B.5}$$

This equation can be simplified to be

$$t_{f,n} = \frac{\delta_T^2}{\alpha_f} \tag{B.6}$$

(iv) $t_{f,b}$

For heat convection in the boundary layer, those terms on the right-hand side of equation (3.12) become negligibly small, giving

$$\frac{\Delta T}{t_{f,b}} \sim V_{z,BL}\frac{\Delta T}{F_B H} \tag{B.7}$$

where $F_B H$ represents the fraction of the flow length along the wall where the buoyancy force has an effect on the fluid motion, see Figure 3.2(d). The quantity $V_{z,BL}$ is used to represent the z velocity inside the boundary layer. Equation (B.7) can be arranged to write

$$t_{f,b} = \frac{F_B H}{V_{z,BL}} \tag{B.8}$$

(v) $t_{f,z}$

For the diffusion of heat in the core region, the convection terms in equation (3.12) vanish, giving

$$\frac{\Delta T}{t_{f,b}} \sim \alpha_f \frac{\Delta T}{(F_f H)^2} \tag{3.9}$$

where $F_f H$ represents the fraction of the tank height along which the diffusion of heat is significant in the core region, see Figure 3.2(e). A rearrangement of equation (3.9) leads to

$$t_{f,z} = \frac{F_f^2 H^2}{\alpha_f} \tag{3.10}$$

(vi) $t_{f,c}$

For convective flow in the core region, the diffusion terms on the right-hand side of equation (3.12) vanish, yielding

$$\frac{\Delta T}{t_{f,c}} \sim V_z \frac{\Delta T}{F_f H} \tag{3.11}$$

where V_z represents the z velocity in the core region, see Figure 3.2(f). It is anticipated that, in the core region, the displacement of water in the z direction is closely related to the convective motion of water in the boundary region. $F_f H$ can thus be used to represent the displacement in the core region. The time scale for

convection in the core region can be derived by rearranging equation (B.11) as

$$t_{f,c} = \frac{F_B H}{V_z} \tag{B.12}$$

A close examination of the six time-scale expressions derived above reveals that there are three unknowns (δ_T, $V_{z,BL}$, V_z) in these expressions. These three unknowns must be expressed in terms of known quantities before the time scales can be calculated. Use is thus made of the continuity equation, the momentum equation, and the energy equation in the boundary layer

$$\frac{\partial V_z}{\partial z} + \frac{\partial V_r}{\partial r} = 0 \tag{B.13}$$

$$V_z \frac{\partial V_z}{\partial z} + V_r \frac{\partial V_z}{\partial r} = \nu_f \frac{\partial^2 V_z}{\partial r^2} + g\beta(T - T_\infty) \tag{B.14}$$

$$V_z \frac{\partial T}{\partial z} + V_r \frac{\partial T}{\partial r} = \alpha_f \frac{\partial^2 T}{\partial r^2} \tag{B.15}$$

In these equations, the length scales r and z may be expressed as δ_T and $F_B H$, respectively. As expected, $F_B H$ is much greater than δ_T.

The continuity equation (B.13) can be used to derive

$$\frac{V_{z,BL}}{F_B H} \sim \frac{V_r}{\delta_T} \tag{B.16}$$

From the energy equation (B.15), one can derive two relations

$$V_{z,BL}\frac{\Delta T}{F_B H} \sim \alpha_f \frac{\Delta T}{\delta_T^2} \tag{B.17}$$

$$V_f \frac{\Delta T}{\delta_T} \sim \alpha_f \frac{\Delta T}{\delta_T^2} \tag{B.18}$$

From equation (B.17) gives

$$V_{z,BL} \sim \frac{\alpha_f F_B H}{\delta_T^2} \tag{B.19}$$

The momentum equation (B.14) can be used to balance the viscous force and the bouyency force in the boundary layer [58]. It follows that

$$g\beta\Delta T \sim \nu_f \frac{V_{z,BL}}{\delta_T^2} = \frac{\alpha_f \nu_f F_B H}{\delta_T^4} \tag{B-20}$$

A slight rearrangement of this equation gives

$$\delta_T = \left(\frac{\alpha_f \nu_f F_B H}{g\beta\Delta T}\right)^{\frac{1}{4}} = F_B H\, Ra_{F_B H}^{-\frac{1}{4}} \tag{B.21}$$

From conservation of mass between the boundary layer flow and the flow in the core region gives

$$V_z = \frac{\delta_T}{R_T} V_{z,BL} \tag{B.22}$$

The time-scale expressions given above are now used to study a sample case in which the storage tank is not insulated; it is desired to compare the importance of various heat transfer mechanisms at 60 seconds. The isotherms plotted for this time (Figure 6.1(a)) are used to evaluate

$$F_s = \frac{1}{2}$$

$$F_f = \frac{1}{3} \qquad (6.23)$$

$$F_g = \frac{1}{3}$$

Other data are listed as follows:

$$\alpha_w = 1.16\times10^{-5}\ m^2/s$$

$$\alpha_f = 1.576\times10^{-7}\ m^2/s$$

$$\alpha_g = 8.27\times10^{-8}\ m^2/s \qquad (6.24)$$

$$\nu_f = 6.67\times10^{-7}\ m^2/s$$

$$\beta_f = 3.6\times10^{-4}\ K^{-1}$$

$$H = 0.3\ m$$

$$R_i = 0.15\ m$$

$$\delta = 0.004\ m$$

$$\Delta T = 10°C$$

With the use of these data for input in equations (8.19), (8.21) and (8.22), values for δ_T, $V_{z,BL}$, and V_z can be estimated as

$$\delta_T = 8.85X10^{-4} \text{ m}$$

$$V_{z,BL} = 4.02X10^{-2} \text{ m/s} \qquad (8.25)$$

$$V_z = 2.37X10^{-4} \text{ m/s}$$

In contrast, the computed results are

$$\delta_T = 5\% \text{ of } R_j = 7.5X10^{-3} \text{ m}$$

$$V_{z,BL} = 3.8X10^{-3} \text{ m/s (maximum)} \qquad (8.27)$$

$$V_z = 5.6X10^{-4} \text{ m/s (maximum)}$$

There is a difference of one order of magnitude between the estimated δ_T and the computed δ_T, and also between the estimated $V_{z,BL}$ and the computed $V_{z,BL}$. However, the estimation of V_z appears satisfactory.

Introducing the estimated values of δ_T, $V_{z,BL}$, and V_z into the time-scale expressions gives

$$t_{w,z} = 7.76X10^{3} \text{ seconds} \qquad t_{a,z} = 1.09X10^{6} \text{ seconds}$$

$$t_{w,r} = 1.38 \text{ seconds} \qquad t_{a,r} = 193.47 \text{ seconds}$$

$$t_{f,n} = 4.37 \text{ seconds} \qquad (8.28)$$

$t_{f,b}$ = 4.97 seconds

$t_{f,z}$ = 2.54×10^{5} seconds

$t_{f,c}$ = 8.44×10^{2} seconds

Some comments can be made based on the time-scale values calculated here.

(i) $t_{w,r} \ll t_{w,z}$

This relation implies that conduction in the z-direction in the wall is much slower than conduction in the r direction in the wall. The temperature distribution in the wall is primarily determined by the conduction in the z direction.

(ii) $t_{f,n} = t_{f,b}$

This relation implies that conduction and convection are equally important in the boundary layer.

(iii) $t_{f,c} \ll t_{f,z}$

This relation implies that in the core region heat diffusion is much slower than heat convection, only convection is important in the core region.

(iv) $t_{w,z} \ll t_{f,z}$ and $t_{w,z}/t_{f,c} = 0.18$

Heat diffusion in the core region is a much slower process than heat conduction in the wall in the z direction. Heat convection in the core region, however, is only about an order of magnitude faster than the heat conduction in the wall in the z direction.

(v) $t_{f,n}/t_{f,c} = t_{f,h}/t_{f,c} \ll 1$

Heat convection in the core region is a much slower process than either the heat conduction across, or the heat convection in, the boundary layer. Heat transfer in the boundary layer is virtually unaffected by the heat transfer in the core region.

The analysis made above can also be extended to study heat transfer in an insulated tank.

(vi) $t_{w,r} < t_{f,n} \ll t_{ins,r}$

Heat transfer across the thickness of the insulation is much slower than either conduction across the tank wall or convection across the boundary layer. Heat transfer in the radial direction is thus controlled mainly by the thermal resistance in the insulation.

(vii) $t_{w,z} << t_{a,z}$ and $t_{w,z} + 2t_{w,r} + 2t_{a,r} << t_{f,z} << t_{a,z}$

In the z direction heat conduction in the insulation is much slower than heat conduction in the wall. The second relation signifies that, if the insulation is placed inside, it is much faster for the heat transfer to take the route of conduction in the z direction in the wall than either conduction in the z direction in the insulation or diffusion of heat in the core region.

(viii) $t_{w,r} + t_{f,n} << t_{a,r}$

Here the relation implies that, when the insulation is placed outside, the time required for the heat to transfer across the boundary layer and wall is much faster than the heat to transfer across the insulation. Using this relation together with the first relation given in (vii) above, one may conclude that the heat will leak more conveniently through the tank wall than through the insulation outside.

REFERENCES

1. Ostrech, S., "Natural Convection in Enclosures," Advances in Heat Transfer, Vol. 8, pp. 161-227, Academic Press, New York, 1972.

2. Catton, I., "Natural Convection in Enclosures," Proceedings of the Sixth International Heat Transfer Conference, Vol. 6, pp. 13-31. McGraw-Hill, New York, 1978.

3. Batchelor, G.K., "Heat Transfer by Free Convection across a Closed Cavity between Vertical Boundaries at Different Temperatures," Quarterly of Applied Mathematics, Vol. 12, pp. 209-233, 1954.

4. Eckert, E.R.G., and Carlson, W.O., "Natural Convection in an Air Layer Enclosed between Two Vertical Plates with Different Temperatures," International Journal of Heat and Mass Transfer, Vol. 2, pp. 106-120, 1961.

5. Elder, J.W., "Laminar Free Convection in a Vertical Slot," Journal of Fluid Mechanics, Vol. 23, pp. 77-98, 1965.

6. Gill, A.E., "The Boundary-Layer Regime for Convection in a Rectangular Cavity," Journal of Fluid Mechanics, Vol. 26, pp. 515-536, 1966.

7. Schinkel, W.M.M., Linthorst, S.J.M., and Hoogendoorn, C.J., "The Stratification in Natural Convection in Vertical Enclosures," Journal of Heat Transfer, Vol. 105, pp. 267-272, 1983.

8. Bohn, M.S., Kirkpatrick, A.T., and Olson, D.A., "Experimental Study of Three-Dimensional Natural Convection High-Rayleigh Number," Journal of Heat Transfer, Vol. 106, pp. 339-345, 1984.

9. Gdalevich, L.B., Nogotov, E.F., and Fertman, V.E., "Effect of Side Walls on Heat Transfer through a Vertical Air Layer in Laminar Natural Convection," International Journal of Heat and Mass Transfer, Vol. 22, pp. 1601-1606, 1979.

10. Meyer, B.A., Mitchell, J.W., and El-Wakil, M.M., "The Effect of Thermal Wall Properties on Natural Convection in Inclined Rectangular Cells," Journal of Heat Transfer, Vol. 104, pp. 111-117, 1982.

11. Elsherbiny, S.M., Hollands, K.G.T., and Raithby, G.D., "Effect of Thermal Boundary Conditions on Natural Convection in Vertical and Inclined Air Layers," Journal of Heat Transfer, Vol. 104, pp. 515-520, 1982.

12. Kim, D.M., and Viskanta, R., "Study of the Effects of Wall Conductance on Natural Convection in Differently Oriented Square Cavities," Journal of Fluid Mechanics, Vol. 144, pp. 153-176, 1984.

13. Morrison, G.L., and Tran, V.Q., "Laminar Flow Structure in Vertical Free Convective Cavities," International Journal of Heat and Mass Transfer, Vol. 21, pp. 202-213, 1978.

14. Mallinson, G.D., and Vahl Davis, G. De, "Three-Dimensional Natural Convection in a Box: A Numerical Study," Journal of Fluid Mechanics, Vol. 83, pp. 1-31, 1977.

15. Schwind, R.G., and Vliet, G.C., "Observations and Interpretations of Natural Convection and Stratification in Vessels," Proceedings of 1964 Heat Transfer and Fluid Mechanics Institute, pp. 51-68, Stanford University Press, Stanford, 1964.

16. Evans, L.B., Raid, R.C., and Drake, E.M., "Transient Natural Convection in a Vertical Cylinder," AIChE Journal, Vol. 14, pp. 251-259, 1968.

17. Hess, C.F., and Miller, C.W., "An Experimental and Numerical Study on the Effect of the Wall in a Thermocline-Type Cylindrical Enclosure-II Numerical Model," Solar Energy, Vol. 28, pp. 153-161, 1982.

18. Hess, C.F., and Miller, C.W., "An Experimental and Numerical Study on the Effect of the Wall in a Thermocline-Type Cylindrical Enclosure-I Experiments," Solar Energy, Vol. 28, pp. 145-152, 1982.

19. Barakat, H.Z., and Clark, J.A., "Analytical and Experimental Study of the Transient Laminar Natural Convection Flow in Partially Filled Liquid Containers," Proceedings of the Third International Heat Transfer Conference, Vol. 2, pp. 152-162, The Science Press, Ephrata, 1966.

20. Sakurai, T., and Matsuda, T., "A Temperature Adjustment Process in a Boussinesq Fluid via a Buoyancy-Induced Meridional Circulation," Journal of Fluid Mechanics, Vol. 54, pp. 417-421, 1972.

21. Jischke, M.C., and Ooty, R.T., "Linearized Buoyant Motion in a Closed Container," Journal of Fluid Mechanics, Vol. 71, pp. 729-754, 1975.

22. Lunde, P.J., Solar Thermal Engineering, John Wiley & Sons, New York, 1980.

23. Close, D.J., "A Design Approach for Solar Processes," Solar Energy, Vol. 11, pp. 112-122, 1967.

24. Gutierrez, G., Hincapie, F., Duffie, J.A., and Beckman, W.A., "Simulation of Forced Circulation Water Heaters, Effects of Auxiliary Energy Supply, Load Type and Storage Capacity," Solar Energy, Vol. 15, pp. 287-298, 1974.

25. Wu, S.T., and Han, S.M., The Numerical and Experimental Studies of Liquid Storage Tank Thermal Stratification for a Solar Energy System, DOE Report No. DOE/CS/34479-3, U.S. Department of Energy, Washington, D.C., 1980.

26. Cabelli, A., "Storage Tanks--A Numerical Experiment," Solar Energy, Vol. 15, pp. 45-54, 1977.

27. Shu, W.T., and Lin, E.I.H., "Three Dimensional Mathematical Model of Flow Stratification in Thermocline Storage Tanks," Application of Solar Energy, Proceedings of the Third Southeastern Conference on Application of Solar Energy, pp. 185-202, University of Alabama in Huntsville Press, Huntsville, 1978.

28. Sharp, M.K., and Loehrke, R.I., "Stratified Versus Well-Mixed Sensible Heat Storage in a Solar Space Heating Application," ASME Paper No. 78-HT-49, 1978.

29. Veltkemp, W.B., "Thermal Stratification in Heat Storages," Thermal Storage of Solar Energy, Proceedings of International TNO Symposium, pp. 47-58, Martinus Nijhoff Publishers, London, 1981.

30. Cole, R.L., and Bellinger, F.O., Natural Thermal Stratification in Tanks Phase 1 Final Report, Argonne National Laboratory Report No. ANL-82-5, Argonne, 1982.

31. Viskanta, R., and Hale, N.W., Jr., "Free Convection Circulation in a Thermal Energy Storage System Driven by Heat Loss from the Walls," Proceedings of the Fourteenth Southeastern Seminars on Thermal Sciences, pp. 25-43, North Carolina State University, Rayleigh, 1978.

32. Jelurie, Y., and Gupta, S.K., "Decay of Thermal Stratification in a Water Body for Solar Energy Storage," Solar Energy, Vol. 28, pp. 137-143, 1982.

33. Gross, R.J., "An Experimental Study of Single Medium Thermocline Thermal Energy Storage," ASME Paper No. 82-HT-53, 1982.

34. Lavan, Z., and Thompson, J., "Experimental Study of Thermally Stratified Hot Water Storage Tanks," Solar Energy, Vol. 19, pp. 519-524, 1977.

35. Sherman, C., Wood, B.D., and Mason, J., "Effect of Vertical Wall Conduction on Temperature Relaxation in Thermally Stratified Liquid Thermal Storage Tanks," SUN II, Proceedings of International Solar Energy Society, pp. 591-595, Pergamon Press, New York, 1979.

36. Miller, C.W., "Effect of a Conducting Wall on a Stratified Fluid in a Cylinder," Heat Transfer and Thermal Control Systems, Progress in Astronautics and Aeronautics, Vol. 60, pp. 190-208, 1977.

37. Chaney, S.R., Humphrey, J.A.C., Monin, L., and Shah, A., "Flow and Heat Transfer of a Stably-Stratified Fluid through an Enclosure," Journal of Solar Energy Engineering, Vol. 106, pp. 261-270, 1984.

38. Jaluria, Y., Natural Convection Heat and Mass Transfer, Pergamon Press, New York, 1980.

39. Sparrow, E.M., and Gregg, J.L., "Similar Solutions for Free Convection from a Nonisothermal Vertical Plate," Journal of Heat Transfer, Vol. 80, pp. 379-386, 1958.

40. Karvinen, R., "Natural and Forced Convection Heat Transfer from a Plate Fin," International Journal of Heat and Mass Transfer, Vol. 24, pp. 881-884, 1981.

41. Kelleher, M., and Yang, K.T., "A Görtler-Type Series for Laminar Free Convection along a Nonisothermal Vertical Plate," Quarterly Journal of Mechanics and Applied Mathematics, Vol. 25, pp. 445-457, 1972.

42. Kao, T.T., Domoto, G.A., and Elrod, H.G., Jr., "Free Convection along a Nonisothermal Vertical Flat Plate," Journal of Heat Transfer, Vol. 99, pp. 72-79, 1977.

43. Na, T.Y., "Numerical Solution of Natural Convection Flow Past a Nonisothermal Vertical Flat Plate," Applied Science Research, Vol. 33, pp. 519-543, 1978.

44. Raithby, G.D., and Hollands, K.G.T., "A General Method of Obtaining Approximate Solutions to Laminar and Turbulent Free Convection Problems," Advances in Heat Transfer, Vol. 11, pp 265-315, Academic Press, New York, 1975.

45. Cebeci, T., "Laminar-Free-Convective-Heat Transfer from the Outer Surface of a Vertical Slender Circular Cylinder," Proceedings of Fifth International Heat Transfer Conference, Vol. 3, pp. 15-19, Japan Society of Mechanical Engineers, Tokyo, 1974.

46. Patankar, S.V., Numerical Heat Transfer and Fluid Flow, Hemisphere Publishing, Washington, D.C., 1980.

47. Sparrow, E.M., and Tao, W.Q., "Buoyancy-Driven Fluid Flow and Heat Transfer in a Pair of Interecting Vertical Parallel Channels," Numerical Heat Transfer, Vol. 5, pp. 39-56, 1982.

48. Parmentier, E.M., and Torrance, K.E., "Kinematically Consistent Velocity Fields for Hydrodynamic Calculations in Curvilinear Coordinates," Journal of Computational Physics, Vol. 19, pp. 404-417, 1975.

49. Kühlbeck, K., Merker, G.P., and Straub, J., "Advanced Numerical Computation of Two-Dimensional Time-Dependent Free Convection in Cavities," International Journal of Heat and Mass Transfer, Vol 23, pp. 203-217, 1980.

50 Andersen, D.A., Tannehill, J.C. and Pletcher, R.H., Computational Fluid Mechanics and Heat Transfer, McGraw-Hill, New York, 1984.

51. Peaceman, D.W., and Rachford, H.H., "The Numerical Solution of Parabolic and Elliptic Differential Equations," Journal of Society Industrial and Applied Mathematics, Vol. 3, pp. 26-41, 1955.

52. Roache, P.J., Computational Fluid Dynamics, Hermosa Publishers, Albuquerque, 1976.

53. Israeli, M., "A Fast Implicit Numerical Method for Time Dependent Viscous Flows," Studies in Applied Mathematics, Vol. 49, pp. 327-349, 1970.

54. Israeli, M., "On the Evaluation of Iteration Parameters for the Boundary Vorticity," Studies in Applied Mathematics, Vol. 51, pp. 67-71, 1972.

55. Roache, P.J., "Semidirect Calculation of Steady Two- and Three-Dimensional Flows," Proceedings of the First International Conference on Numerical Methods in Laminar and Turbulent Flows, pp. 17-27, Wiley, New York, 1978.

56. Elchhorn, R., "Natural Convection in a Thermally Stratified Fluid," Progress in Heat and Mass Transfer, Vol. 2, pp. 41-53, Pergamon Press, New York, 1969.

57. Jaluria, Y., "Natural Convection Flow in a Stratified Medium," Proceedings of International Conference on Numerical Methods in Thermal Problems, pp. 433-443, Pineridge Press, England, 1979.

58. Bejan, A., Convection Heat Transfer, John Wiley & Sons, New York, 1984.

59. Cheesewright, R., "Natural Convection from a Plane, Vertical Surface in Non-Isothermal Surroundings," International Journal of Heat and Mass Transfer, Vol. 10, pp. 1847-1859, 1967.

60. Yang, K.T., Novotny, J.L., and Cheng, Y.S., "Laminar Free Convection from a Nonisothermal Plate Immersed in a Temperature Stratified Medium," International Journal of Heat and Mass Transfer, Vol. 15, pp. 1097-1109, 1972.

61. Fujii, T., Takenchi, M., and Morioke, I., "Laminar Boundary Layer of Free Convection in a Temperature Stratified Environment," Proceedings of the Fifth International Heat Transfer Conference, Vol. 3, pp. 44-48, Japan Society of Mechanical Engineers, Tokyo, 1974.

62. Chan, C.C., and Eichhorn, R., "Natural Convection from a Vertical Surface to a Thermally Stratified Fluid," Journal of Heat Transfer, Vol. 98, pp. 446-451, 1976.

63. Jaluria, Y., and Himasekhar, K., "Buoyancy-Induced Two-Dimensional Vertical Flows in a Thermally Stratified Environment," Computer and Fluids, Vol. 11, pp. 39-48, 1983.

64. Bontoux, P., Gilly, B., and Roux, B., "Analysis of the Effect of Boundary Conditions on Numerical Stability of Solutions of Navier-Stokes Equations," Journal of Computational Physics, Vol. 36, pp. 417-427, 1980.

65. Petterson, J., and Imberger, J., "Unsteady Natural Convection in a Rectangular Cavity," Journal of Fluid Mechanics, Vol. 100, pp. 65-86, 1980.

66. Humphrey, J.A.C., "Some Scales Relavent to Thermocline Degradation," Appendix IV, Experimental and Theoretical Study of Thermocline Degredation, Final Report, University of California, Berkeley, 1982.

BIOGRAPHICAL SKETCH

Ruey-Jong Shyu was born on February 12, 1953, in Tainan, Taiwan, Republic of China. He graduated from the National Tsing-Hua University in June 1975, with a Bachelor of Science degree in nuclear engineering. After two year's military service, he served as research and teaching assistant in the Nuclear Engineering Department of the Tsing-Hua University. In September 1979, he entered the University of Florida and received a Master of Science degree in mechanical engineering in August 1981. Since then, he has studied for the Doctor of Philosophy degree in the same department.

In July 1981, he married Miss Chia-Jo Huang, who has two degrees, a Master of Science in industrial and systems engineering and a Master of Science in mathematics, both from the University of Florida.

I certify that I have read this study and that in my opinion it conforms to acceptable standards of scholarly presentation and is fully adequate, in scope and quality, as a dissertation for the degree of Doctor of Philosophy.

C.K. Hsieh, Chairman
Professor of Mechanical Engineering

I certify that I have read this study and that in my opinion it conforms to acceptable standards of scholarly presentation and is fully adequate, in scope and quality, as a dissertation for the degree of Doctor of Philosophy.

C.T. Hsu
Professor of Engineering Sciences

I certify that I have read this study and that in my opinion it conforms to acceptable standards of scholarly presentation and is fully adequate, in scope and quality, as a dissertation for the degree of Doctor of Philosophy.

R.A. Gater
Associate Professor of Mechanical Engineering

I certify that I have read this study and that in my opinion it conforms to acceptable standards of scholarly presentation and is fully adequate, in scope and quality, as a dissertation for the degree of Doctor of Philosophy.

E.C. Hansen
Assistant Professor of Mechanical Engineering

I certify that I have read this study and that in my opinion it conforms to acceptable standards of scholarly presentation and is fully adequate, in scope and quality, as a dissertation for the degree of Doctor of Philosophy.

Tom I.P. Shih
Assistant Professor of Mechanical Engineering

This dissertation was submitted to the Graduate Faculty of the College of Engineering and to the Graduate School and was accepted as partial fulfillment of the requirements for the degree of Doctor of Philosophy.

August, 1985

Robert A. Bare
Dean, College of Engineering

Dean, Graduate School